Chapter 3

Functionalized Imidazolium-Based Permanganate Organic-Inorganic Hybrid as Internal Oxidative Catalyst for Controlled Oxidation of Benzyl Alcohols

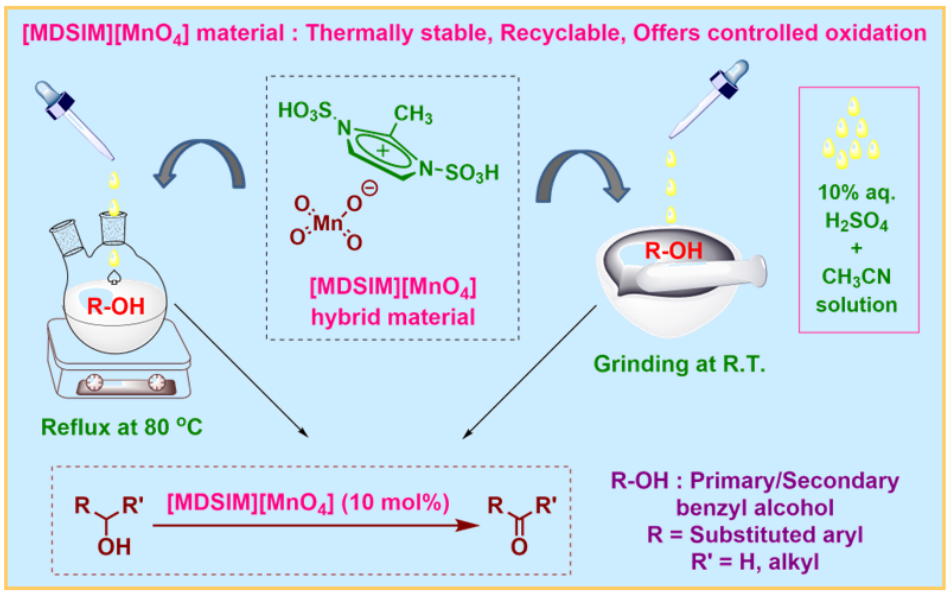

Synopsis

In this study, an organic-inorganic hybrid 2-methyl-1,3-disulfoimidazolium permanganate ([MDSIM][MnO_4]) was prepared as a solid material *via* ion exchange reaction of 2-methyl-1,3-disulfoimidazolium chloride ([MDSIM]Cl) ionic liquid with potassium permanganate at room temperature. Various spectroscopic and analytical techniques like FT-IR, UV-Vis DRS, PXRD, Raman, SEM, EDX and elemental mapping studies were used to confirm the structural composition of this hybrid. The extensive thermal stability of the hybrid was indicated by thermo-gravimetric analysis, whereas SEM images pointed out the heterogeneous morphology of various sized crystalline granules. Oxidative efficiency of the material was investigated as recyclable homogeneous catalyst for controlled oxidation of primary/secondary benzyl alcohols to carbonyl compounds in 10% aqueous H_2SO_4 and acetonitrile solution at 80 ºC and in solvent-drop grinding method at room temperature in presence of an acidic co-catalyst. Theoretical calculations using density functional theory (DFT), regarding the optimized structure of the hybrid and proposed mechanism of oxidation reaction, also provided support towards the efficacy of this recyclable material as catalyst as well as oxidant.

3.1. Introduction

Selective oxidation of primary/secondary alcohols to aldehydes/ketones represents an important intervening step in synthetic organic chemistry to produce biologically active molecules and synthetically prime substrates [1, 2]. The most favourable parameters of such oxidants include non-toxic and non-corrosive nature, high rate of product conversion without side product formation, use of stoichiometric amounts of reagents, mild conditions and compatibility with different functional groups.

Potassium permanganate represents a strong non-selective metal-based oxidant used for oxidation of alcohols to carbonyl compounds or acids either acidic, basic or neutral aqueous solution [1, 3, 4]. But from the observed limitations of $KMnO_4$ for alcohol oxidation [5, 6] in water, as discussed under **sub-unit 1A.5.1 (Chapter 1A)**, it is clear that modification of the permanganate oxidant is required to eliminate difficulties related to the solubility of organic substrate, increasing stability of the oxidant in water with control on the oxidizing power as well as catalytic use of the modified oxidant. Using phase transfer catalysts, the non-selective behaviour of $KMnO_4$ oxidant has been improved as compared to the acidic and basic conditions with raising solubility of the

organic substrates [7-9]. Nevertheless, this synthetic approach also causes over-oxidation of primary alcohols, leading to acidic product formation [10]. For example, Jose and co-workers employed 18-crown-6 as a phase-transfer catalyst to improve the solubility of $KMnO_4$ in benzene in a solid-liquid system, which yielded benzaldehyde as sole product for benzyl alcohol oxidation. Yet, formation of benzoic acid was also observed when temperature and catalyst amount were raised [9]. Another modification of the reactivity of $KMnO_4$ has been done by supporting the oxidant on solid supports which include $KMnO_4/CuSO_4.5H_2O$ [11], $KMnO_4/MnO_2$ [12], $KMnO_4$/montmorillonite K10 [13], $KMnO_4/ZrOCl_2.8H_2O$ [14], $KMnO_4$/Graphite [15], $KMnO_4$/silica gel [16], $KMnO_4$/aluminium silicate [17], $KMnO_4$/kieselguhr reagent [18] etc. However, most of these methods used excess amount of $KMnO_4$/solid support reagents because of incompetent nature of these systems in the oxidation reactions. The use of ionic liquid as greener solvent has been observed to increase the selective oxidative capacity of $KMnO_4$ in 1-butyl-3-methylimidazolium tetrafluoroborate [bmim][BF_4] ionic liquid using equivalent amount of the reagent at ambient temperature for alcohol oxidation [19]. Safaei-Ghomi *et al.* employed 1-butyl-3-methylimidazolium bromide [bmim][Br] ionic liquid mixed CH_3CN for the same purpose with lesser amount of the $KMnO_4$ oxidant [20]. Jasim *et al.* developed combination of [TAIm][MnO_4]/[TAIm][OH] as recyclable triazine based oxidative ionic liquids system containing 1,1',10"-(1,3,5-triazine-2,4,6-triyl)tris(3-methyl-1*H*-imidazol-3-ium) ([TAIm]$^+$) as organic cation for gram scale selective aerobic oxidation of alcohols under mild homogeneous conditions [21].

Subsequently, organic-inorganic hybrid materials have been developed by incorporation of permanganate anion into the organic cations, that enhanced performances of individual units while lowering their drawbacks and thereby, such materials found extensive applications in the field of oxidation as well as dihydroxylation of olefins [22]. These include examples of quaternary ammonium and phosphonium permanganates as oxidants [23, 24], as discussed in **Chapter 1, sub-unit 1A.5.1**. In this regard, cetyltrimethylammonium permanganate (CTAP) worked as a potent oxidant for *cis*-hydroxylation of alkenes [23, 24] and oxidation of pharmaceutically significant drug ingredient carbamezpine (CBZ) [25]. It was also used for oxidative regeneration of carbonyl compounds from several aldo- or keto-oximes [24, 26]. Likewise, tetrabutylammonium permanganate (TBAP) was prepared as non-selective oxidant for conversion of various organic substrates to acids such as aromatic aldehydes, benzyl alcohols, p-nitrotoluene and *cis*-stilbene at room temperature in

pyridine [27]. Still, the use of quaternary ammonium and phosphonium permanganates persisted an issue to conduct any oxidation at high temperature [28], with their explosive nature at higher temperature [29].

In this situation, there is an urgent need to design a sustainable organic-inorganic permanganate hybrid of higher thermal stability, good solubility in organic solvent and controlled selectivity, which can be used as catalyst for controlled oxidation of organic substrates at mild conditions. Such type of permanganate hybrid can be designed through incorporation of sulfonic acid functionalized organic cation with the permanganate anion by ion-exchange reactions of ionic liquids with the permanganate anion. This may lead to tight binding of the organic cation with the anion by extensive intramolecular H-bonding interactions involving the -OH group of sulfonic acid and the oxygen atoms of MnO_4^- anion, as compared to the earlier reported ammonium-based permanganate hybrids without functional groups present [23-27]. Furthermore, the sulfonic groups of organic cations in the hybrid would generate a chain of intermolecular H-bonds among the individual hybrid molecules and might contribute significant amount of thermal stability to the material. The existence of acidic groups in the hybrid can also modify the oxidative power of permanganate ions as well as hydrophobic/hydrophilic properties.

In continuation of the development of task-specific ionic liquid based organic-inorganic hybrid material for catalytic applications [30, 31], herein it was aimed to synthesize N-SO_3H group tethered 2-methyl-1,3-disulfoimidazolium ($[MDSIM]^+$) cation-based permanganate organic-inorganic hybrid [MDSIM][MnO_4], as per reaction **Scheme 3.1**, through ion-exchange reaction of a reported precursor ionic liquid [MDSIM]Cl with aqueous $KMnO_4$ solution. By confirming the structures of permanganate hybrid using spectroscopic and other analytical techniques, their oxidative properties were investigated as recyclable homogeneous catalyst for controlled oxidation of primary/secondary benzyl alcohols to aldehydes/keto compounds (**Scheme 3.2**) in presence of dilute sulfuric acid as co-catalyst in polar organic solvent mixture at different temperatures as well as in solvent-drop grinding method [32, 33]. The room temperature solvent-drop grinding method in these reactions was expected to provide a milder approach to the reactions in solution under reflux temperature. Besides the experimental works, theoretical calculations were done to get information about the optimized structure of the hybrid as well as the feasibility of proposed reaction scheme in terms of thermodynamics.

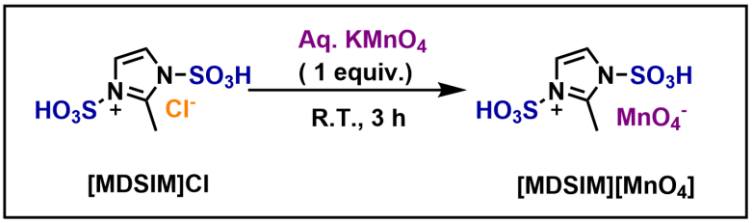

Scheme 3.1: Synthesis of hybrid permanganate salt of sulfonic acid functionalized 2-methylimidazolium cation.

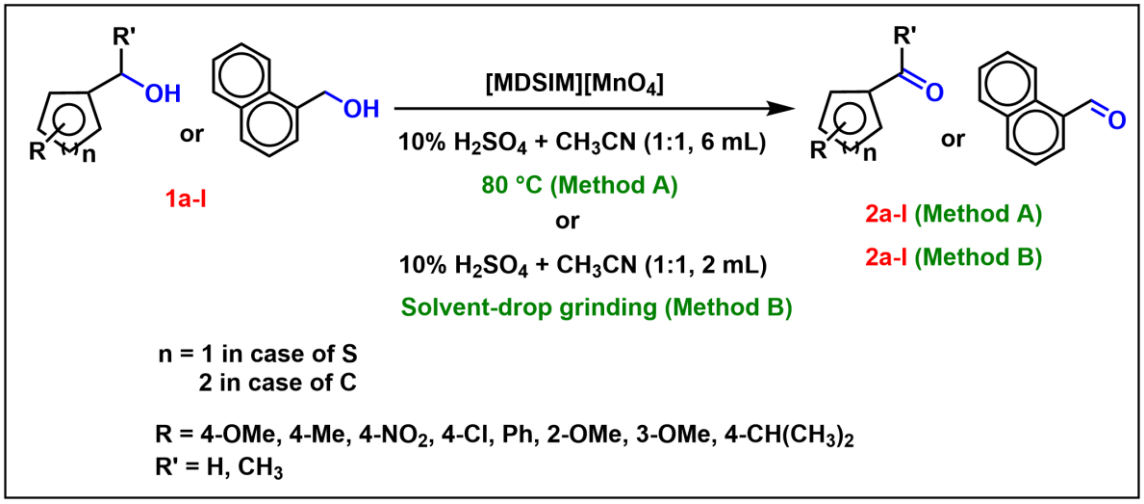

Scheme 3.2: Selective oxidation of aromatic alcohols by the synthesized permanganate salt under heating conditions (**Method A**) and solvent-drop grinding conditions (**Method B**).

3.2. Results and Discussion

3.2.1. Catalyst characterization

The solid material, synthesized according to **Scheme 3.1**, was characterized through various analytical techniques.

3.2.1.1. NMR and FT-IR analyses

Although, the heterogeneous nature of IL-permanganate hybrid in NMR solvents, including $CDCl_3$, DMSO-d_6, CD_3OD and D_2O, restricted to take ^1H and ^{13}C NMR spectra of the organic cation, but the existence of 2-methyl-1,3-disulfoimidazolium cation in this hybrid could be supported from ^1H and ^{13}C NMR spectra of the precursor ionic liquid [MDSIM]Cl (**section 3.4.3**) [34]. Additionally, the comparative FT-IR spectra also evidenced the incorporation of organic cation into the synthesized

permanganate salt by indicating characteristic peaks of sulfonic groups attached to the organic cation (**Fig. 3.1a**).

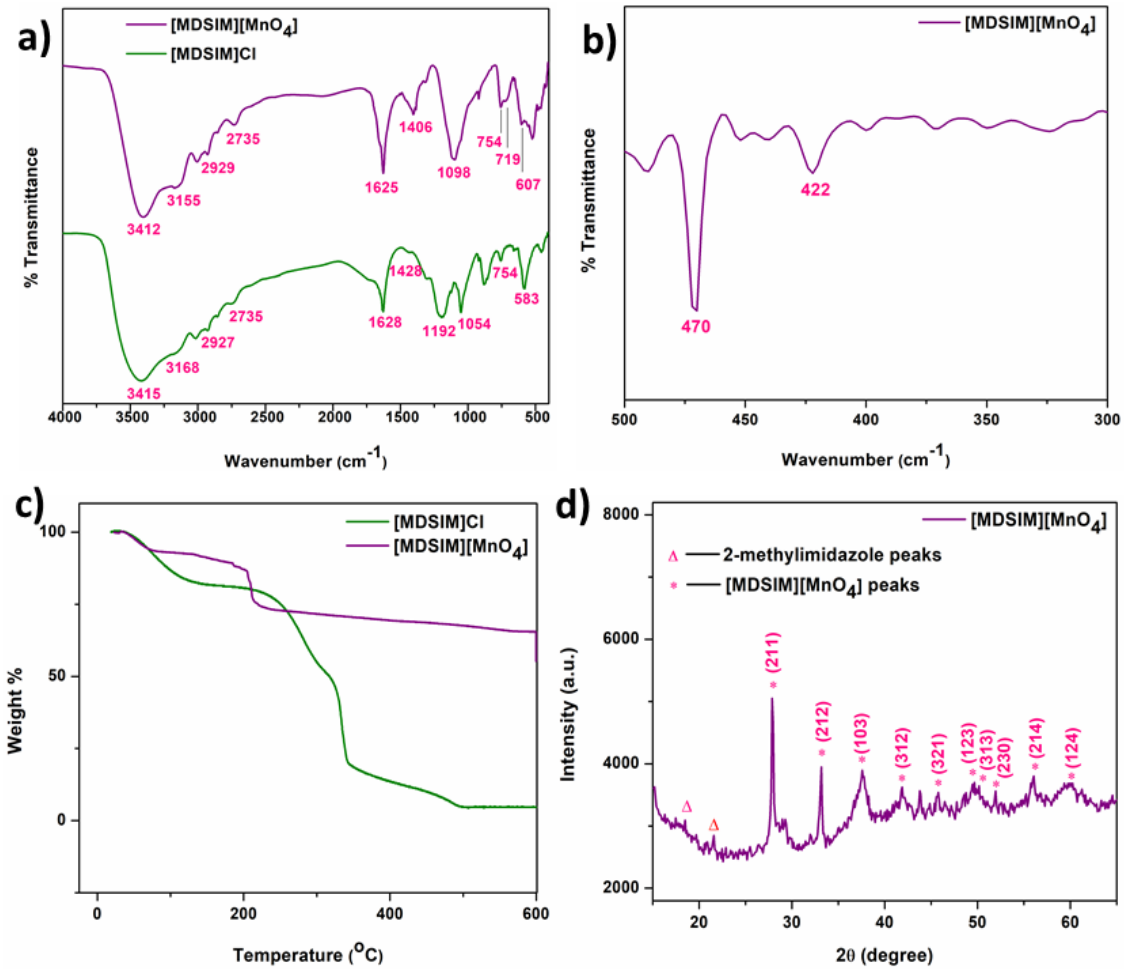

Fig. 3.1: a) FT-IR spectrum of synthesized [MDSIM][MnO_4] compared to parent IL [MDSIM]Cl; b) Far IR spectrum of [MDSIM][MnO_4]; c) Thermogravimetric analysis curve of [MDSIM][MnO_4]; d) Powder-XRD patterns of [MDSIM][MnO_4] hybrid.

The attachment of -SO_3H group to the organic cation of [MDSIM]Cl ionic liquid could be recognized from prominent absorption peaks of S-O asymmetric and symmetric stretch at 1192 cm^{-1} and 1054 cm^{-1} respectively, along with S-O bending vibration at 583 cm^{-1}. As compared to the parent ionic liquid, IR spectrum of the IL-permanganate hybrid showed only one strong vibration for S-O stretch at 1098 cm^{-1} and another weak S-O bending vibration at 607 cm^{-1} which evidenced the existence of SO_3H group in the organic cation. Peaks at 1406 cm^{-1} and 719 cm^{-1} could be assigned as out of plane ring bending of C-H bond and bending vibrations of -CH_3 group, respectively. Medium strength peak at 754 cm^{-1} could be expected from N-S stretching vibration. Broad peaks

around 3155-3412 cm^{-1} could be attributed to O-H stretch of -SO_3H group as well as physisorbed water molecules. The sharp peak at 1625 cm^{-1} expressed bending vibration of water molecules along with overlapped C=C stretch of imidazolium ring. The methyl group C-H stretch was observed around 2929 cm^{-1} and 2735 cm^{-1}. The unique peak of permanganate ion at 910 cm^{-1} could be identified as overlapping with the strong peak of hybrid around 1098 cm^{-1} region as IR-active vibration, in contrast to its inactive nature in the Raman spectrum (**Fig. 3.4b**) of permanganate hybrid [35, 36]. To further confirm the presence of permanganate ion in the hybrid, its Far-IR region was analysed (**Fig. 3.1b**) which showed two distinct vibrations as medium to weak peaks around 500-400 cm^{-1} corresponding to ν_4 (F_2) Raman active mode as per literature [36].

3.2.1.2. Thermogravimetric analysis

Thermogravimetric analysis of the organic salt, [MDSIM][MnO_4] showed two degradation slopes in the thermogram, one nearby 100 °C and another around 200 °C (**Fig. 3.1c**). The first mass loss of 6.7% up to 100 °C could be accounted for elimination of physisorbed water and this amount was found to be equal to 1 equivalent of water. The 2nd decomposition of the dehydrated permanganate organic salt around 200 °C could be expected from disintegration of weaker Mn-O bond present in the hybrid to form molecular oxygen. A total weight loss of approximately 16% occurred up to this temperature which provided evidence for two equivalents of dioxygen evolution under thermal condition. As reported, the thermal decomposition of $KMnO_4$ shows similar weight loss at 250 °C (in air) for emission of the oxygen gas [37]. This implied a weakening of the Mn-O bonds in the anionic part of [MDSIM][MnO_4] due to existence of weaker interactions between the imidazolium cation and permanganate anion compared to the strong ionic bond of K^+ cation and the permanganate anion, which would need high temperature to cleave the Mn-O bonds. On comparing the thermogram of the parent chloride ionic liquid, it showed more hygroscopic nature by weight loss of around 16% of physisorbed water below 100 °C than the hybrid permanganate salt.

3.2.1.3. Powder X-Ray Diffraction analysis

The powder X-ray diffraction pattern of [MDSIM][MnO_4] (**Fig. 3.1d**) displayed the primitive lattice structure of the organic hybrid salt, which was retained as that of precursor $KMnO_4$. The XRD pattern of hybrid showed that the intensity of peaks at higher 2θ values decreased after the replacement of K^+ cation with bulkier sulfonic acid

functionalized imidazolium cation. The most intense peak of $KMnO_4$ at 27.78° for reflection plane (211), as per JCPDS card no. 89-3951, could be assigned to 2θ value of the hybrid at 27.86°. The other 2θ values such as 33.17°, 37.56°, 41.86°, 45.75°, 49.01°, 50.19°, 51.95°, 55.98° and 59.34° could be attributed to reflection planes of (212), (103), (312), (321), (123), (313), (230), (214) and (124) respectively.

3.2.1.4. Scanning Electron Microscopy analysis

Two of the SEM images of permanganate hybrid (**Fig. 3.2a & Fig. 3.2b**) expressed its heterogeneous surfaces with different sized crystalline structures. The morphological patterns of SEM images displayed nearly medium sized crystals to agglomerate shapes. The average size of the granules was around 1.395 μm. The formation of aggregates within the system expressed existence of some intermolecular interactions in the hybrid. The heterogeneity of the material might be an effect of $-SO_3H$ groups attached with the imidazolium cation of hybrid that possess H-bonding capacity, which led to the formation of extensive H-bonded lump of [MDSIM][MnO_4] molecules. The presence of two highly polarised $-SO_3H$ groups in each imidazolium cation possibly formed exceedingly linked chains of molecules, holding tightly onto each other through intermolecular H-bonding. Apart from that, a probable sharing of charge of the oxygens of permanganate anion between two imidazolium rings through H-bonding, ion-ion and ion-dipole like interactions might also assembled the particles to its high rigidity (**Fig. 3.2c**), that could only be cluttered using acid solution at elevated temperatures.

3.2.1.5. Energy Dispersive X-Ray analysis

The Energy Dispersive X-ray (EDX) image identified all the desired elements present in the organic salt (**Fig. 3.3a**) without appearance of any other element or impurities. Over the same surface, elemental mapping of all the possible elements were done which revealed the active metal centres distributed thoroughly on the surface (**Fig. 3b-f**).

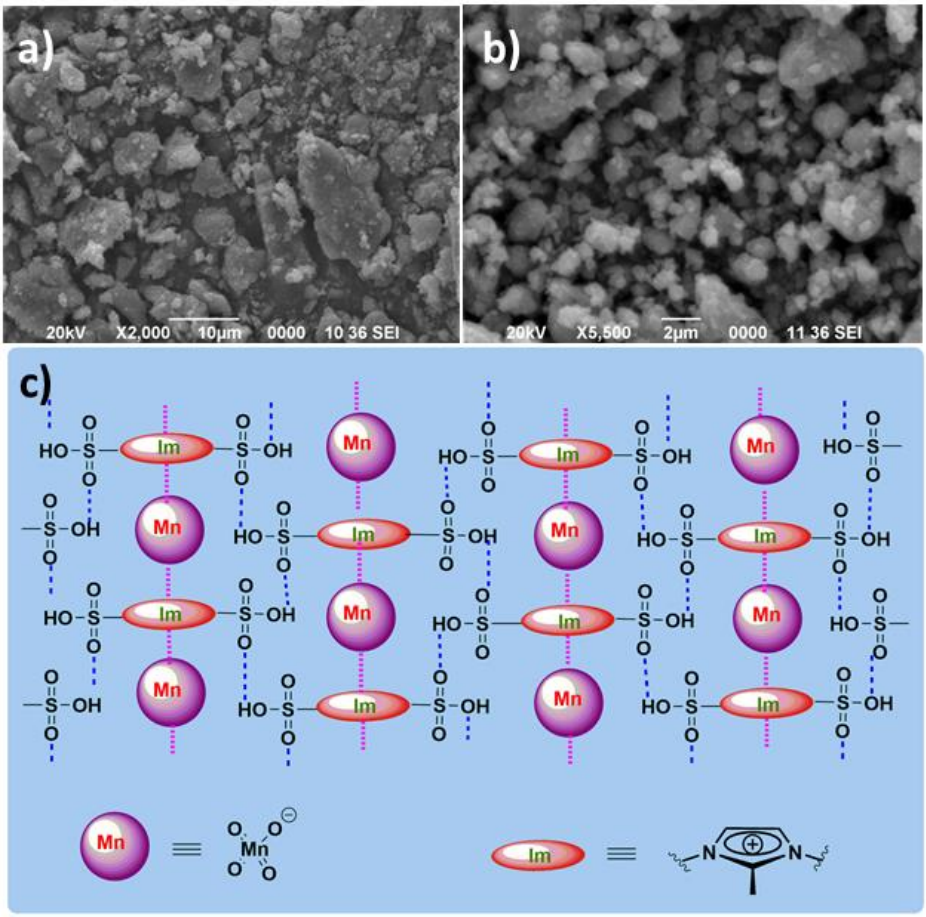

Fig. 3.2: a-b) SEM images of [MDSIM][MnO_4]; c) plausible interactions among groups and ions of [MDSIM][MnO_4].

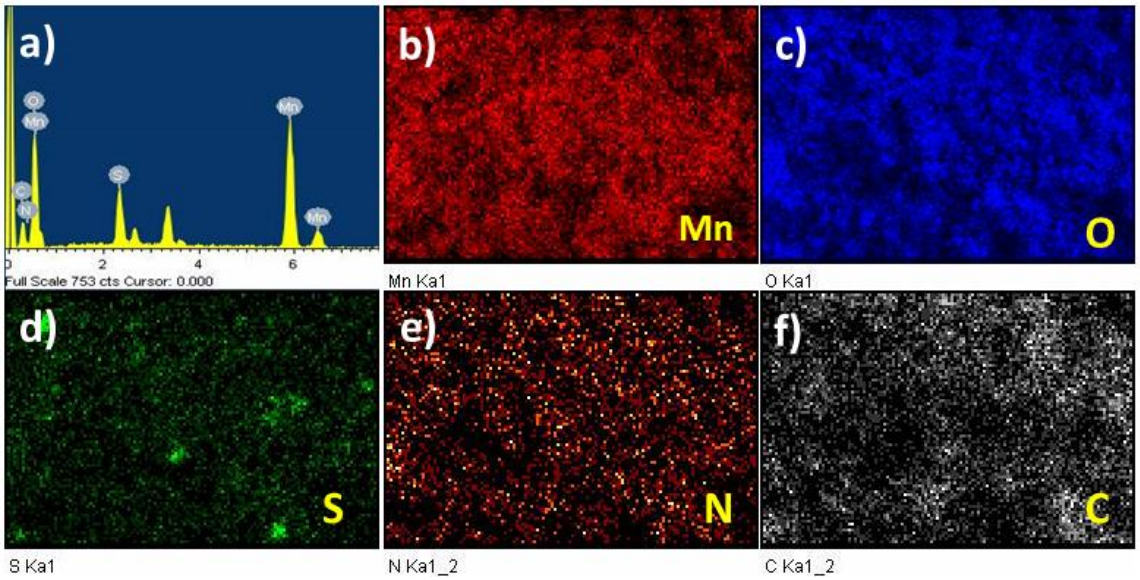

Fig. 3.3: a) EDX analysis of [MDSIM][MnO_4]; Elemental mapping of [MDSIM][MnO_4] constituent elements b) Mn c) O d) S e) N f) C.

3.2.1.6. UV-Vis Diffuse Reflectance Spectra analysis

The UV-Vis DRS spectrum of [MDSIM][MnO_4] (**Fig. 3.4a**) was compared to that of $KMnO_4$ (**section 3.4.4**). The [MDSIM][MnO_4] spectrum showed two distinct absorptions of permanganate ion around 222 nm and 311 nm in the hybrid, which could be attributed to $^1A_1 \rightarrow {}^1T_2$ ($t_1 \rightarrow 4t_2$) and $^1A_1 \rightarrow {}^1T_2$ ($3t_2 \rightarrow 2e$) electronic transitions respectively [38]. The medium intensity absorption peak observed for $KMnO_4$ around 540 nm was broaden in the hybrid as weak shoulders around 545 nm, corresponding to $^1A_1 \rightarrow {}^1T_2$ ($t_1 \rightarrow 2e$) electronic transition. Apart from these three allowed transitions, the orbitally forbidden $^1A_1 \rightarrow {}^1T_1$ ($3t_2 \rightarrow 2e$) transition caused weak absorbances around 347 nm and 365 nm in $KMnO_4$ and the hybrid, respectively. However, another weak absorbance around 690 nm in $KMnO_4$ corresponding to $^1A_1 \rightarrow {}^1T_1$ ($t_1 \rightarrow 2e$) forbidden transition was not distinct in case of the synthesized material. As compared to the UV-Vis DRS spectrum of $KMnO_4$, the intensities of peaks in that of [MDSIM][MnO_4] around 365 nm and 545 nm were seen to be significantly reduced. This might be because the electronic states of permanganate ion became diverse within the hybrid by virtue of inter/intra-molecular H-bonding interactions of -SO_3H groups attached to imidazolium cation with the oxygen atoms of permanganate anion in the hybrid as shown in **Fig. 3.2c**. These secondary interactions of the permanganate ion were lacked in case of $KMnO_4$, as the electronic states were discrete in presence of smaller K^+ cation in $KMnO_4$ [39]. DFT study of the optimized structure also evidenced existence of various ionic and weak interactions in the hybrids.

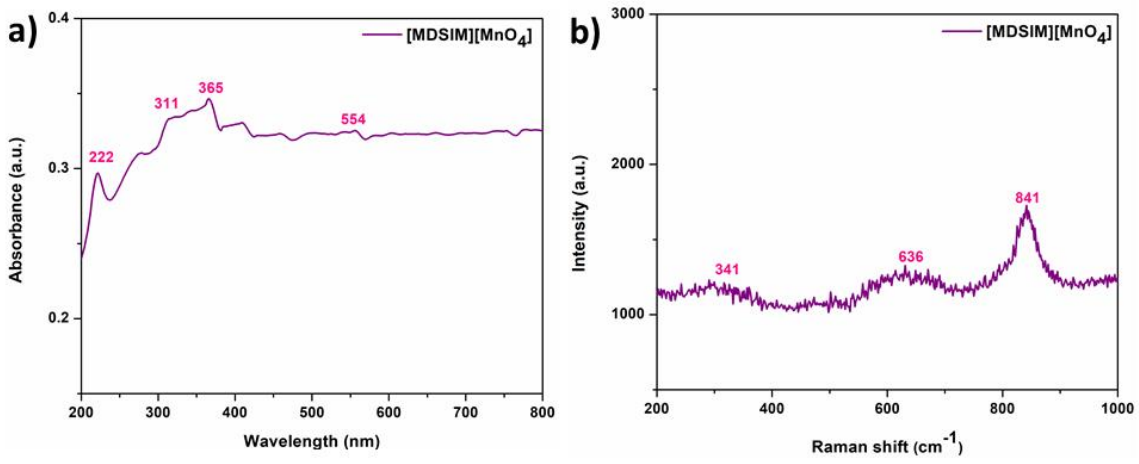

Fig. 3.4: a) UV-Vis DRS spectrum of [MDSIM][MnO_4]; b) Raman spectrum of [MDSIM][MnO_4] hybrid.

3.2.1.7. Raman analysis

The Raman spectrum of [MDSIM][MnO_4] hybrid (**Fig. 3.4b**) displayed characteristic Raman active peak of permanganate ion at 841 cm^{-1} corresponding to "breathing'' symmetric mode ν_1 (A_1), which was observed at 836 cm^{-1} in the Raman spectrum of $KMnO_4$ (**section 3.4.4**) [40]. The position of this peak in the hybrid was slightly changed along with reduction in peak intensity as compared to that in the spectrum of $KMnO_4$. But the hybrid did not show the weak peak around 910 cm^{-1} for ν_3 (F_2) vibrational modes of MnO_4^- moiety. This could be because of the distortion of regular tetrahedral structure of MnO_4^- in the hybrid for plausible intra/inter-molecular ionic and H-bonding interactions, as observed in DFT study, within the hybrid owing to the sulfonic acid functionalized imidazolium cation in place of K^+ cation. Again, the IR active weak vibration of the permanganate ion related to ν_4 (F_2) vibrational mode around 500-400 cm^{-1}, as shown by the Far-IR spectrum of hybrid (**Fig. 3.1b**), was reported to be very weak Raman active peak in the literature [36]. However, the broad weak peak at 341 cm^{-1} in the Raman spectrum of hybrid could be correlated to the ν_2 (E) weak peak of $KMnO_4$ at 386 cm^{-1}. Additionally, another weak impurity peak was observed at 636 cm^{-1} for MnO_2 which might be present in small amount with the hybrid.

3.2.2. Solubility study of permanganate hybrid

Several polar and non-polar solvents were used to identify the solubility of permanganate hybrid. It was found that the compound was partially soluble in polar organic solvent (*t*-BuOH, CH_3CN, CH_3COCH_3), but insoluble in water and non-polar solvents ($CHCl_3$, CH_2Cl_2, $C_6H_5CH_3$). The partial solubility of permanganate hybrid was also observed in water through addition of dilute sulfuric acid solution. This solubility was further increased by combining dilute sulfuric acid (10% aqueous H_2SO_4) with polar organic solvents such as acetonitrile, acetone and *t*-butyl alcohol in 1:1 ratio at high temperature.

3.2.3. Catalytic study

The oxidative nature of permanganate-based imidazolium hybrid was investigated for conversion of substituted primary/secondary aromatic alcohols to aldehyde/keto compounds using varied amount of the permanganate hybrid in acidic solution of polar organic solvents at different temperatures. For these studies, 4-

methoxybenzyl alcohol was selected as model substrate to determine the optimized amount of oxidative catalyst, solvent system and reaction temperature.

3.2.3.1. Optimization of reaction conditions

Solvent effects on the oxidation of 4-methoxybenzyl alcohol (**1a**) was examined by treatment of 1 mmol of **1a** with 10 mol% of [MDSIM][MnO_4] in acidic solution of *t*-BuOH, CH_3CN and CH_3COCH_3 at different pH under reflux conditions (**Table 3.1).** The reaction did not occur in CH_3CN under neutral condition at 80 °C (or room temperature) in heterogeneous phases (**Table 3.1, entry 1**). A trace amount of product was formed in 10% aqueous H_2SO_4 solution (pH 1) in 5 h reaction time at 100 °C without acetonitrile solvent (**Table 3.1, entry 2**). Interestingly, when the same reaction was conducted in 1:1 mixture of 10% sulfuric acid and CH_3CN solution (pH 1) at 80 °C, it showed 92% conversion of starting compound with selective formation of 4-methoxybenzaldehyde (**2a**, 86% yield) (**Table 3.1, entry 3**) during 3 h reaction. This surmised involvement of the acid as a co-catalyst in the oxidation reaction. Upon further diluting the acidic solution of CH_3CN to pH 3-4, the reaction did not proceed even after 6 h at 80 °C (**Table 3.1, entry 4**). Both *tert*-butyl alcohol and acetone displayed better results when mixed in 1:1 ratio with 10% H_2SO_4 solution for this oxidation reaction under reflux at pH 2 (**Table 3.1, entries 5-6**). Performance of this reaction was found to be moderate with 71% yield of product, when the reaction was carried out in 50% acetic acid solution (pH~3) (**Table 3.1, entry 7**). From this study, it was decided to conduct the oxidation in 10% sulfuric acid in CH_3CN solution as suitable reaction medium for optimization of the reaction temperature as **Method A**. The model reaction was also studied in solvent-drop grinding method using mortar and pestle, which produced 82% yield of product within 1 h reaction period (**Table 3.1, entry 8**) using 10-12 drops (2 mL) of 10% aqueous H_2SO_4 and acetonitrile solution (1:1 ratio) in presence of 10 mol% of the hybrid catalyst. This method was further utilized for substrate scope study of alcohols as **Method B**.

Table 3.1: Effects of solvent at different pH on the model product **2a** using 10 mol% of [MDSIM][MnO_4] catalyst.

Entry	Solvent	pH	Temp (°C)	Time (h)	%Conversion[a]	% Yield[b] **2a**
1	CH_3CN	-	80	5	-	-
2	10% H_2SO_4	1	100	5	Trace	-

3	**10% H_2SO_4 + CH_3CN (1:1)**	**1**	**80**	**3**	**92**	**86**
4	dil. H_2SO_4 (0.1 N) + CH_3CN (1:1)	3-4	80	6	-	-
5	10% H_2SO_4 + $(CH_3)_3COH$ (1:1)	2	80	2	89	74
6	**10% H_2SO_4 + Me_2CO (1:1)**	**2**	**50**	**4**	**90**	**84**
7	50% Glacial AcOH	3	80	4	89	71
8	**10% H_2SO_4 + CH_3CN (1:1)[c]**	**1**	**R.T.**	**1**	**90**	**82**

[a] % Conversion was calculated from **Equation 1B.3** (**Chapter 1B, sub-unit 1B.3.14)**; [b] Isolated yield; [c] Under solvent-drop grinding conditions.

From the optimization of solvent effect study, we selected 1:1 mixture of 10% aqueous H_2SO_4 and acetonitrile solution as reaction medium to find the optimized reaction temperature for the model reaction in **Method A** using 10 mol% of the hybrid catalyst at different temperatures i.e. 80 °C, 50 °C and 25 °C. The results were included in **Table 3.2 (entries 1-3)**. At room temperature, the reaction took longer reaction time (5 h) to produce 80% yield of the product (**Table 3.2, entry 1**) as compared to lower reaction time at 50 °C (**Table 3.2, entry 2**). The rate of reaction slowly increased with rising temperature and showed maximum yield at 80 °C in 3 h (**Table 3.2, entry 3**). **Table 3.2** also displayed the results of catalyst amount optimization study for the model reaction with variation of catalyst amount (5, 10 and 15 mol%) in 10% aqueous sulfuric acid and acetonitrile solution at 80 °C. Using 5 mol% of the permanganate-based catalyst gave around 81% yield of product in 4 h (**Table 3.2, entry 4**). Elevating the catalyst amount up to 15 mol% produced almost identical results when 10 mol% catalyst was used (**Table 3.2, entries 5 & 3**). On that account, 10 mol% of the permanganate catalyst was considered for substrate scope study at 80 °C in 10% sulfuric acid and acetonitrile solvent system.

Table 3.2: Optimization of reaction temperature and catalyst amount for the model reaction (**Method A**) using [MDSIM][MnO_4] hybrid.

Entry	Temperature (°C)	Catalyst amount (mol%)	Time (h)	% Conversion[a]	% Yield[b] **2a**
1	R.T.	10	5	83	80
2	50	10	4	89	83
3	**80**	**10**	**3**	**92**	**86**
4	80	5	4	85	81
5	**80**	**15**	**3**	**92**	**86**

[a] % Conversion was calculated from **Equation 1B.3** (**Chapter 1B, sub-unit 1B.3.14)**; [b] Isolated yield: using 1 mmol substrate (**1a**) in 1:1 mixture of 10% aqueous H_2SO_4 and acetonitrile at pH 1.

3.2.3.2. Substrate scope study

The optimized reaction conditions, obtained from oxidation of model substrate 4-methoxybenzyl alcohol in solution (**Method A**) and in solvent-drop grinding method (**Method B**), were implemented on various substituted primary/secondary aromatic alcohols at 80 °C and ambient temperature, respectively. In **Method A** (**Fig. 3.5**), alcohols having electron-donating substituents at *para*-position offered better outcomes while those with electron-withdrawing substituents produced highly selective aldehyde product, although the conversion rates of these alcohols were quite poor. The yields of carbonyl products were observed to be low for alcohols having electron-donating substituents at *ortho*- or *meta*-positions due to steric effects with the permanganate based redox catalyst containing bulkier organic cation. For *sec*-alcohol 1-phenylethanol, the resultant ketone (**2f**) formation was remarkable. Impressive results were obtained for the heterocyclic alcohol 2-thiophenemethanol (**2j**), but alcohols having two phenyl rings brought about appalling outcomes, probably due to steric reason. Overall, moderate to poor % yields of isolated carbonyl products were generated in reactions done by **Method A**. In **Method B** (**Fig. 3.6**), the conversion rates of most alcohols to carbonyl derivatives were not satisfactory, leading to moderate to lower yields of a few products. As compared to the solution reactions, side product formation in grinding reactions was found to be less or none. To monitor the progress of reaction, FT-IR spectra of the crude reaction mixture were recorded after certain interval of time (15 min, 30 min, 45 min, 60

min) which identified the formation of almost pure product within 1 h, in case of the model reaction under **Method B** (**Fig. 3.7**). HPLC spectra of oxidized products of the alcohols formed by **Method A** and **Method B** are given in **section 3.4.5.**

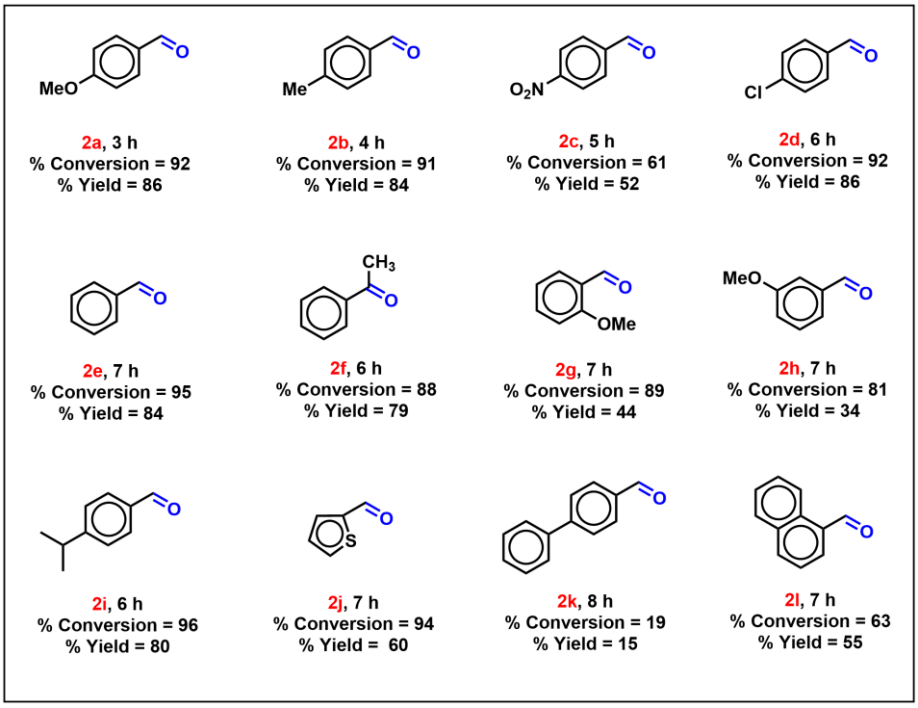

Fig. 3.5: Substrate scope study for the oxidation of alcohols by heating (**Method A)**.

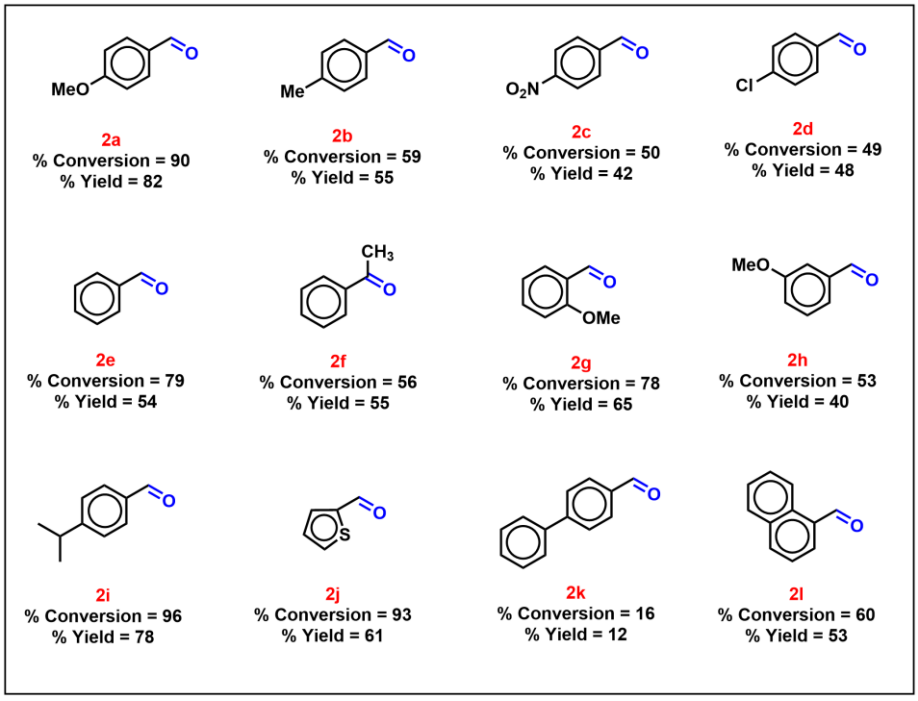

Fig. 3.6: Substrate scope study for the oxidation of alcohols by solvent-drop grinding (**Method B)**.

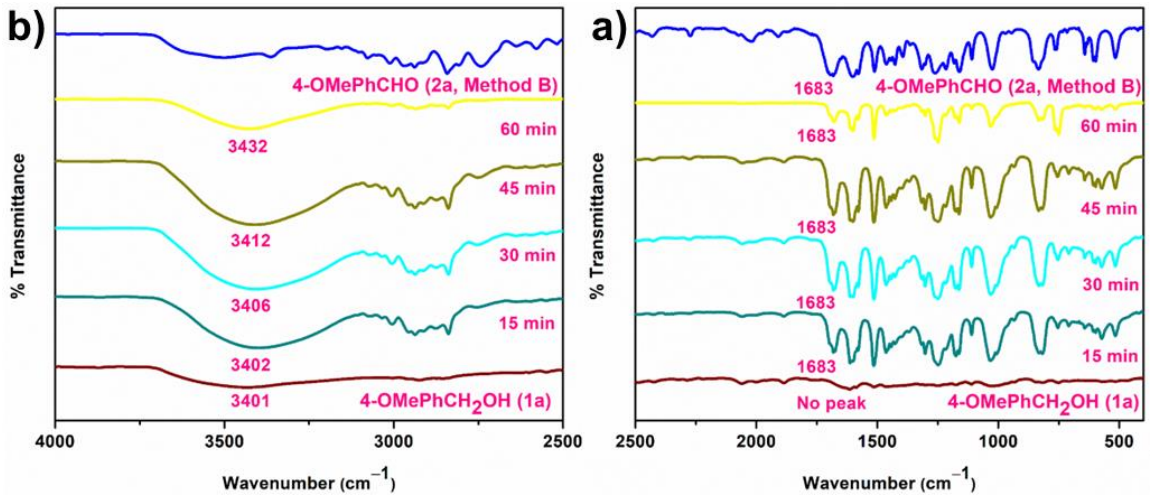

Fig. 3.7: FT-IR spectra of reaction mixture collected over a time range of 0-60 min during the oxidation of 4-methoxybenzyl alcohol (**1a**) by **Method B**, a) FT-IR range 400-2500 cm^{-1}; b) FT-IR range 2500-4000 cm^{-1}.

A comparative table (**Table 3.3**) for some reported oxidants was also included to observe the catalytic activity of the [MDSIM][MnO_4] hybrid for oxidation of benzyl alcohols [41-44, 9, 19].

Table 3.3: Comparison of oxidative ability of some reported oxidants related to oxidation of primary/secondary benzyl alcohols.

Entry	Oxidant [Ref.]	Substrate	Product	Time	Temp (°C)	Yield%
1	Activated MnO_2 (50-100 mg/mmol)/O_2, toluene [41]	Benzyl alcohols	Benzaldehyde	8 h	110	29-99
2	Excess amount of Jones reagent in acetone [42]	Benzyl alcohols	Benzaldehyde	20 min	0	76
3	Aqueous or 50% acetic acid solution of ceric ammonium nitrate (2.5 equivalent per mole) [43]	Benzyl alcohols	Benzaldehyde	2-30 min	50-100	35-94
4	Collins reagent [44] (6 equivalent/mole), CH_2Cl_2	Primary/secondary benzyl alcohols	Aldehydes/ketones	5-15 min	25	87-96
5	Molar equivalent $KMnO_4$, 18-Crown-6 as catalyst, benzene [9]	Benzyl alcohols	Benzaldehydes	2 h	20-70	51 -71
6	Molar equivalent of $KMnO_4$ in	Benzyl alcohols	Aldehydes/ketones	1-2 h	R.T.	83-97

	[bmim]BF_4 ionic liquids [19]					
7	10 mol% [MDSIM][MnO_4] recyclable catalyst in 10% aqueous H_2SO_4 and CH_3CN (1:1) solution (This work)	Benzyl alcohols	Aldehydes/ketones	3-8 h	80	30-86
8	10 mol% [MDSIM][MnO_4] recyclable catalyst, 10% aqueous H_2SO_4 and CH_3CN solution (10-12 drops), Grinding method (This work)	Benzyl alcohols	Aldehydes/ketones	1 h	R.T.	12-82

3.2.3.3. Plausible mechanism

The plausible mechanism of the permanganate salt catalysed oxidation of alcohols can be explained using benzyl alcohol (**1e**) as the model substrate (**Scheme 3.3**). Anionic counterpart of the organic salt is activated by protonation, causing the electron deficient metal centre to undergo co-ordination through π-interaction with the aromatic ring of alcohol. The direct nucleophilic attack by -OH group of alcohol moiety may be obstructed by the cationic imidazolium group, possibly due to steric reasons in intermediate III. The proximity of alcohol to the metal centre compelled the nucleophilic attack of -OH group to the Mn (VII) centre giving coupling complex **IV**, where elimination of hydrogen molecule takes place to generate the carbonyl product. The reproduced hybrid material can further undergo the same oxidation cycle as catalyst as well as oxidant, in the presence of sulfuric acid as co-catalyst.

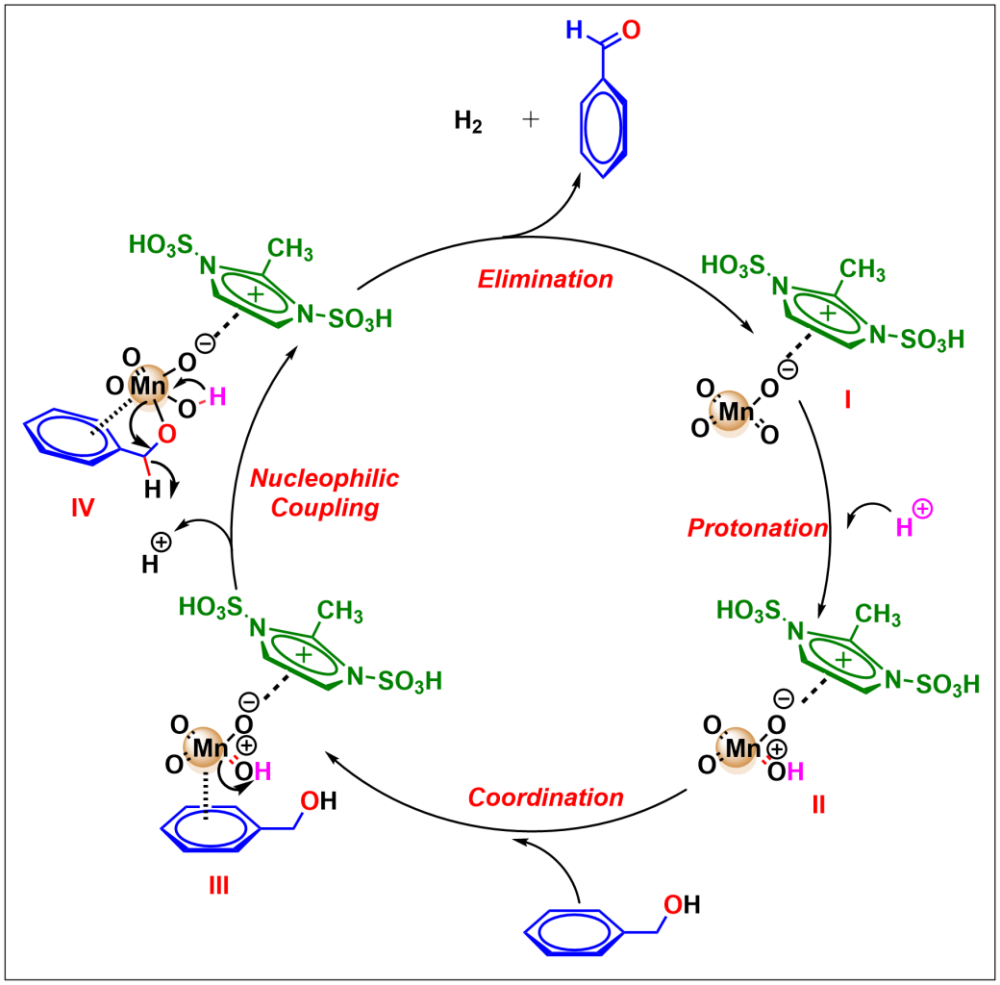

Scheme 3.3: Plausible mechanism for oxidation of aromatic alcohols to carbonyl compounds.

3.2.4. Catalyst recyclability

Recyclability of the oxidative catalyst was studied in 3 mmol scale of model reaction after successfully completing the first run of reaction in 10% sulfuric acid and acetonitrile solution as per the optimized reaction conditions. The used catalyst was recovered from aqueous extract of acidic solution, after isolation of the product, through treatment with 10% aqueous NaOH solution. The alkaline solution was added in slight excess after neutralization for complete precipitation of the organic salt. The solution was then centrifuged, washed with distilled water followed by acetone and the residue was dried in vacuum oven for 24 h.

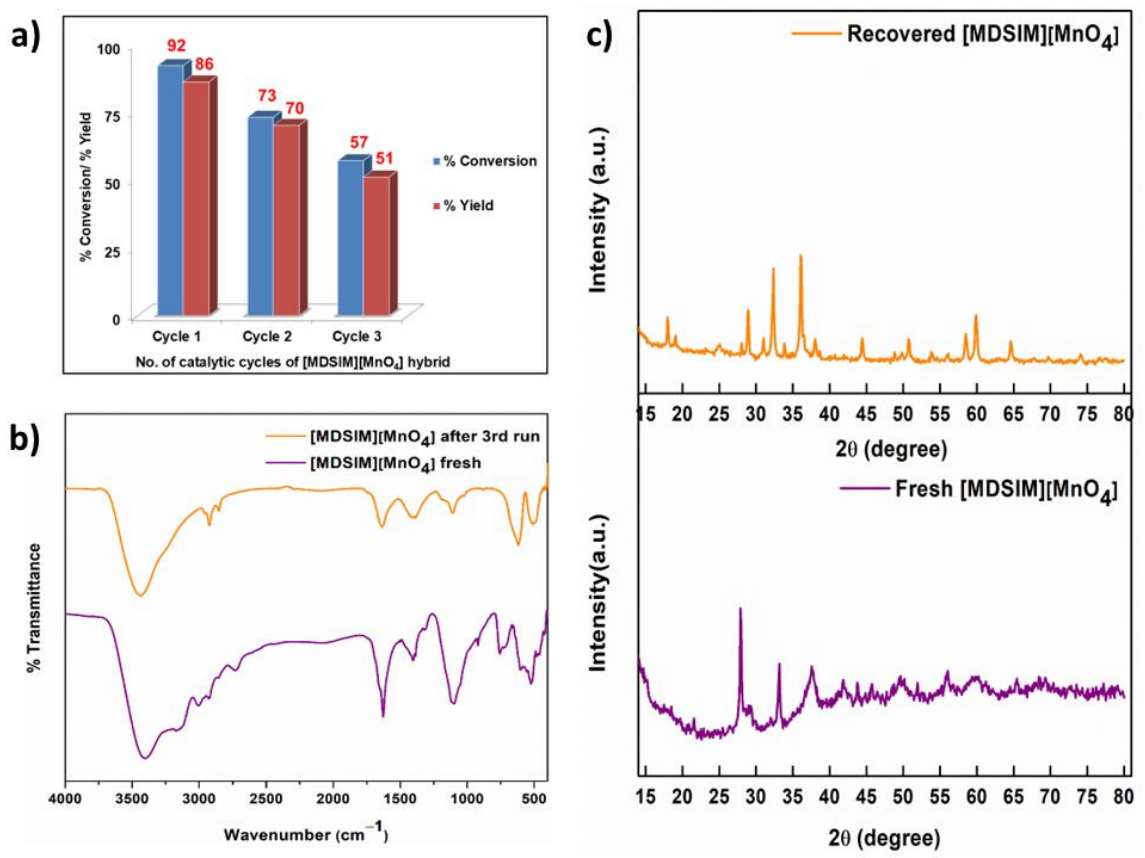

Fig. 3.8: a) Bar diagram for recyclability of catalyst for the model reaction by **Method A** at 3 h; b) comparative FT-IR spectra of fresh catalyst and recycled catalyst; c) P-XRD spectra of fresh and recovered catalyst.

The recovered catalyst was analysed using FT-IR, P-XRD, EDX as well as elemental mapping to confirm the intactness of the salt. Decrease in the outcome of desired product by **Method A** at analogous reaction time for three consecutive run was depicted by **Fig. 3.8a**, which might be because of reduced activity of catalyst due to its frequent washing and reactivation in vacuum. **Fig. 3.8b** showed a comparative FT-IR spectra between a 3rd time recycled catalyst and the fresh one. The powder-XRD pattern of the recovered catalyst displayed most of the peaks exhibited by fresh [MDSIM][MnO_4] with slight shifting of 2θ (degree) values as depicted by **Fig. 3.8c**, which might be due to the slight distortion of tetrahedral structure of MnO_4^-, because of repeated neutralization of the used catalyst with NaOH solution for reactivation process. EDX analysis (**Fig. 3.9a**) and elemental mapping (**Fig. 3.9b-e**) confirmed the presence of all elements in the recovered [MDSIM][MnO_4] material with a homogeneous distribution through the surface.

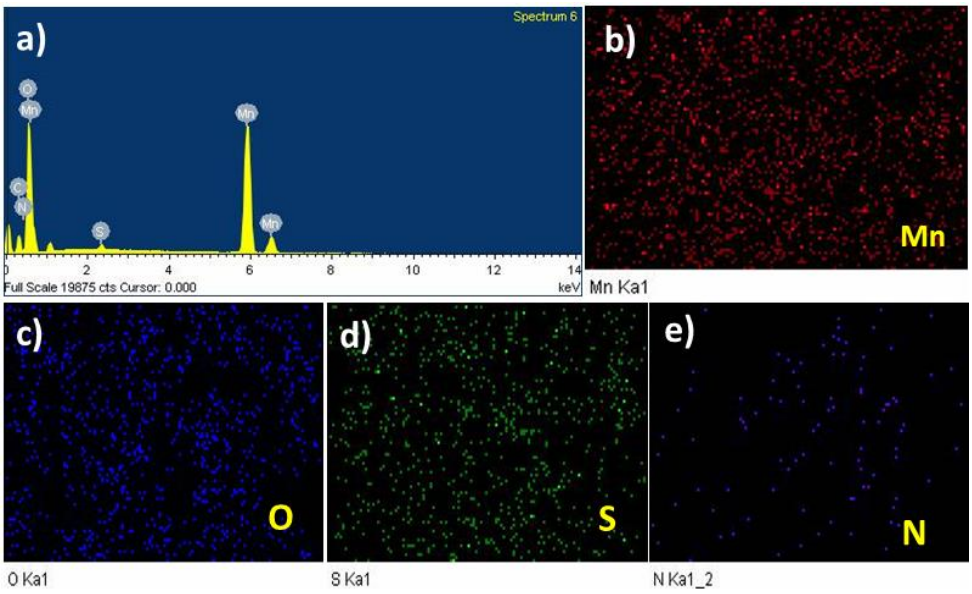

Fig. 3.9: a) EDX analysis of recovered catalyst; Elemental mapping of recovered catalyst constituent elements b) Mn, c) O, d) S, e) N.

3.2.5. DFT calculations

Electronic structures of 2-methyl-1,3-disulfoimidazolium cation $[MDSIM]^+$, permanganate anion (MnO_4^-), reaction intermediates **IM I, IM II, IM III, IM IV**, $C_6H_5CH_2OH$, C_6H_5CHO and H_2 were optimized at gas-phase using the density functional theory (DFT) method [45-49]. The Cartesian coordinates of all the optimized structures were included in **Table 3.A (section 3.4.6)**. Furthermore, real and positive vibration frequency values, observed during frequency calculations of all the optimized species at the same level of theory to obtain different modes of frequencies and thermochemical results, were mentioned in **Table 3.B (section 3.4.6)**.

Firstly, the optimizations of individual ions $[MDSIM]^+$ and MnO_4^- as well as combination of both the ions in the same environment (considering two $[MDSIM]^+$ and two MnO_4^- ions) were done using B3LYP/6-311++G(d,p) level of theory (**Fig. 3.10**). As these species came closer to each other in **Fig. 3.10**, different interactions between O-atom of MnO_4^- with O, N and H-atoms of $[MDSIM]^+$ were noticed. The distance between O24-atom of the MnO_4^- and the N32-atom of $[MDSIM]^+$ ion was found as 3.030 Å, while the O44 atom of other MnO_4^- with the N32 atom of the same $[MDSIM]^+$ was positioned at 3.218 Å. The O23 atom of MnO_4^- was observed at 3.239 Å from the C4-atom of other $[MDSIM]^+$ cation. The optimized structures also displayed formation of H-bond between the H20-atom of one $[MDSIM]^+$ ion and the O37-atom of another

$[MDSIM]^+$ at a distance of 1.638 Å. At the same time, another H-bond formed between the H42-atom of $[MDSIM]^+$ ion and the O44-atom of MnO_4^- with a distance of 1.792 Å. It was also noticed that the H52-atom of one $[MDSIM]^+$ and the H21-atom of another $[MSDIM]^+$ were strongly attracted by the O45 atom of one MnO_4^- and the O24 atom of another MnO_4^-, forming bonds at the distances of 0.997 Å and 0.999 Å, respectively. The distances from H52 atom to the O41 atom of one $[MDSIM]^+$ and H21 atom to the O18 atom of other $[MDSIM]^+$ cation were found as 1.689Å and 1.662Å, respectively.

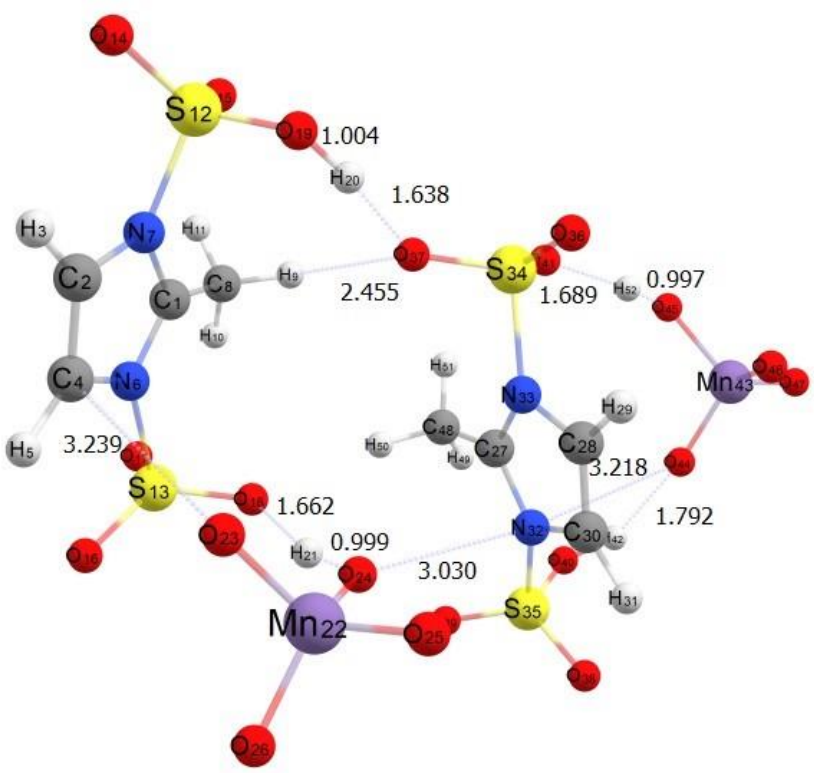

Fig. 3.10: Optimized structure of $[MDSIM][MnO_4]$ at B3LYP/6-311++G(d,p) level of theory.

Fig. 3.11 depicted the optimized electronic structures of all species involved in the proposed oxidative reaction mechanism (**Scheme 3.3**) during experimental study along with some important bond length parameters (in Å) using the same level of theory. To remove the complexities, benzyl alcohol ($C_6H_5CH_2OH$, **1e**) and benzaldehyde (C_6H_5CHO, **2e**) were used to illustrate the proposed mechanistic pathway. In the optimized structure of intermediate **IM I**, we found that MnO_4^- anion was in close vicinity of $[MDSIM]^+$ ion. In this structure, the O26 atom of MnO_4^- was positioned at 2.494 Å from the C1 atom and 2.791 Å from both N6 as well as N7 atoms of the $[MDSIM]^+$ ion. The Mn22-atom and O26 atom of MnO_4^- were found to be 1.624 Å

away from each other. In the next step, formation of **IM II** took place after protonation (H^+) of MnO_4^- anion, where the distances of O26 atom of MnO_4^- from N6, C1 and N7 atoms of $[MDSIM]^+$ ring increased as compared to those in **IM I**. Mn22-O26 bond distance of MnO_4^- in **IM II** was found to be 1.577 Å, which was decreased by 0.047 than that in **IM I.** The reason behind was assumed to be the addition of H^+ to one O atom of the MnO_4^- moiety, which would pull the electron density making other Mn-O bonds shorter. Introduction and subsequent optimization of $C_6H_5CH_2OH$ in the **IM II** environment gave rise to **IM III** intermediate. In **IM III**, the distances of the O26-atom of MnO_4^- from N6, C1 and N7 atoms of $[MDSIM]^+$ ion were slightly decreased as compared to those in **IM II**. The Mn22-O26 bond distance in **IM III** was observed as 1.584 Å which was slightly greater than that in **IM II**. These changes were probably due to the appearance of electron rich aromatic ring of benzyl alcohol. It was further noted that the O24-atom of MnO_4^- was found to be at 1.910 Å with the H40-atom of $C_6H_5CH_2OH$, and at the same time O25 of MnO_4^- was at 2.913 Å, 2.775 Å and 2.656 Å, respectively, from C28-atom, C32-atom and C33-atom of $C_6H_5CH_2OH$ molecule. A weak interaction between Mn22-atom of MnO_4^- and O43-atom of $C_6H_5CH_2OH$ was also observed which is equal to 4.080 Å. However, Mn22-atom of MnO_4^- formed a bond with O43-atom of $C_6H_5CH_2OH$ by nucleophilic coupling, causing the bond distance to be decreased to 2.094 Å in **IM IV**. Lastly, elimination took place and the final compound C_6H_5CHO was formed by the removal of H_2, accompanying the regeneration of **IM I** ([MDSIM][MnO_4]).

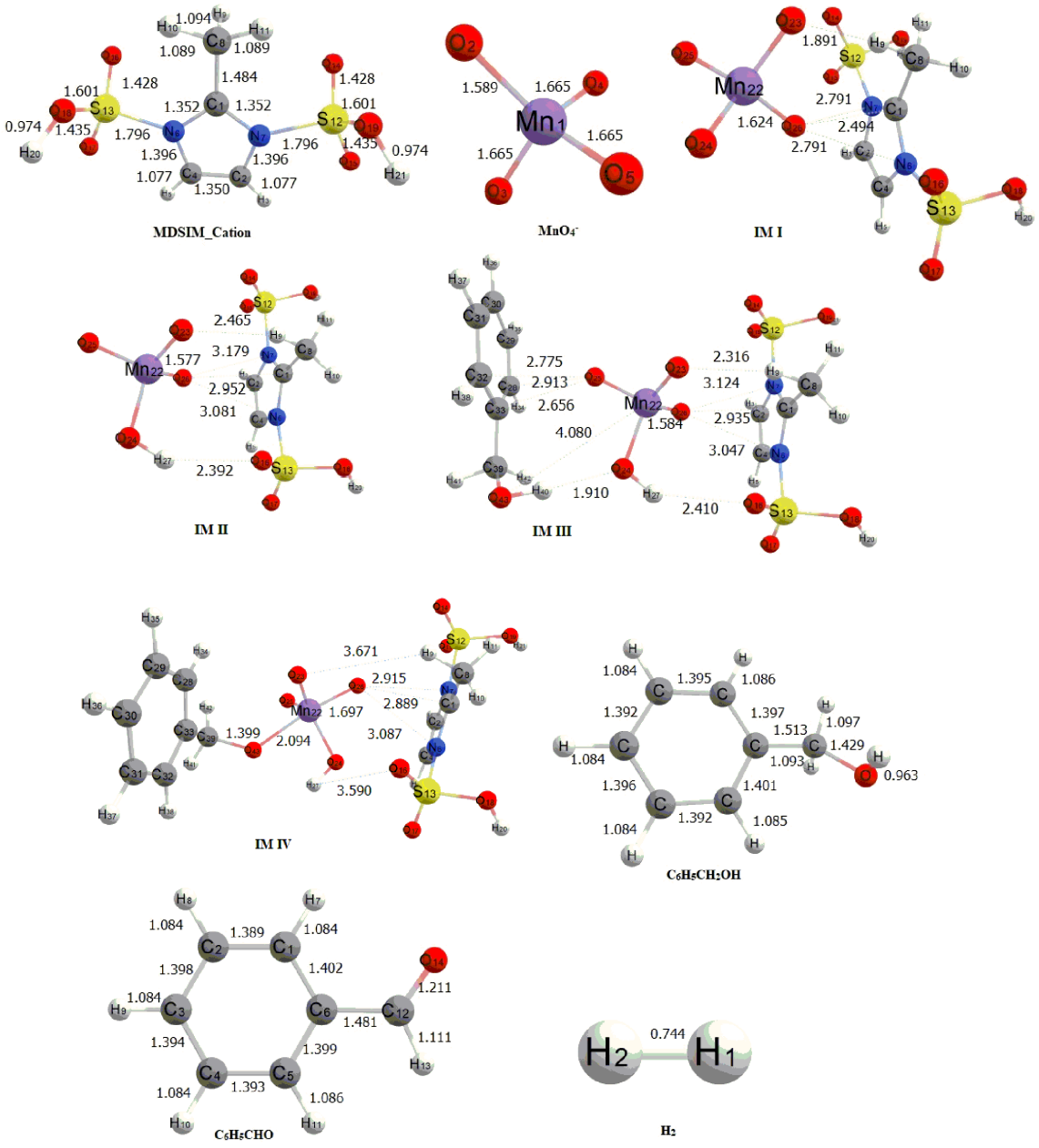

Fig. 3.11: Optimized structures of all species involved in the proposed reaction mechanism of oxidation at B3LYP/6-311++G(d,p) level of theory.

Table 3.C (section 3.4.6) reported the thermo-chemical data, including total energy, enthalpy, and Gibb's free energy of all species that were obtained through frequency calculations. Using **Table 3.C (section 3.4.6)**, the thermodynamic parameters of reaction mechanism such as standard enthalpy change (Δ_rH^o) and Gibb's free energy change (Δ_rG^o) in each reaction step were determined and were included in **Table 3.4**.

Table 3.4: Standard enthalpy and Gibbs free energy changes (in kcal mol^{-1}) of reaction steps at B3LYP/6-311++G(d,p) level of theory.

Reaction Channels	**$\Delta_r H^o$**	**$\Delta_r G^o$**
$[MDSIM]^+ + MnO_4^- \rightarrow$ **IM I**	-79.98	-68.76
IM I + $H^+ \rightarrow$ **IM II**	-235.46	-229.22
IM II + $C_6H_5CH_2OH \rightarrow$ **IM III**	-6.63	4.56
IM III – $H^+ \rightarrow$ **IM IV**	-6.86	-17.69
IM IV$\rightarrow C_6H_5CHO + H_2 +$ **IM I**	259.34	244.94

In the first step, negative values of $\Delta_r H^o$ and $\Delta_r G^o$ were obtained in the formation of intermediate **IM I** when $[MDSIM]^+$ ion interacted with MnO_4^- anion, indicating that this step was exothermic and spontaneous. Protonation of **IM I** into **IM II** in the next step generated more negative values of $\Delta_r H^o$ and $\Delta_r G^o$, implying this step to be highly exothermic and more spontaneous. Formation of **IM III** intermediate in the 3rd step was slightly exothermic and somewhat non-spontaneous. However, getting rid of a proton from **IM III** gave rise to **IM IV** intermediate, revealing the exothermic ($\Delta_r H^o<0$) and spontaneous behaviour ($\Delta_r G^o<0$) of the reaction. The last step (desorption) would be endothermic and non-spontaneous, as it would require energy to eliminate C_6H_5CHO and H_2 from IM IV to regenerate **IM I** intermediate $[MDSIM][MnO_4]$.

With the help of the absolute energy value of each species as given in **Table 3.C (section 3.4.6)**, we explored all reaction species on the potential energy diagram concerning $[MDSIM]^+$ cation and MnO_4^- anion (**Fig. 3.12).**

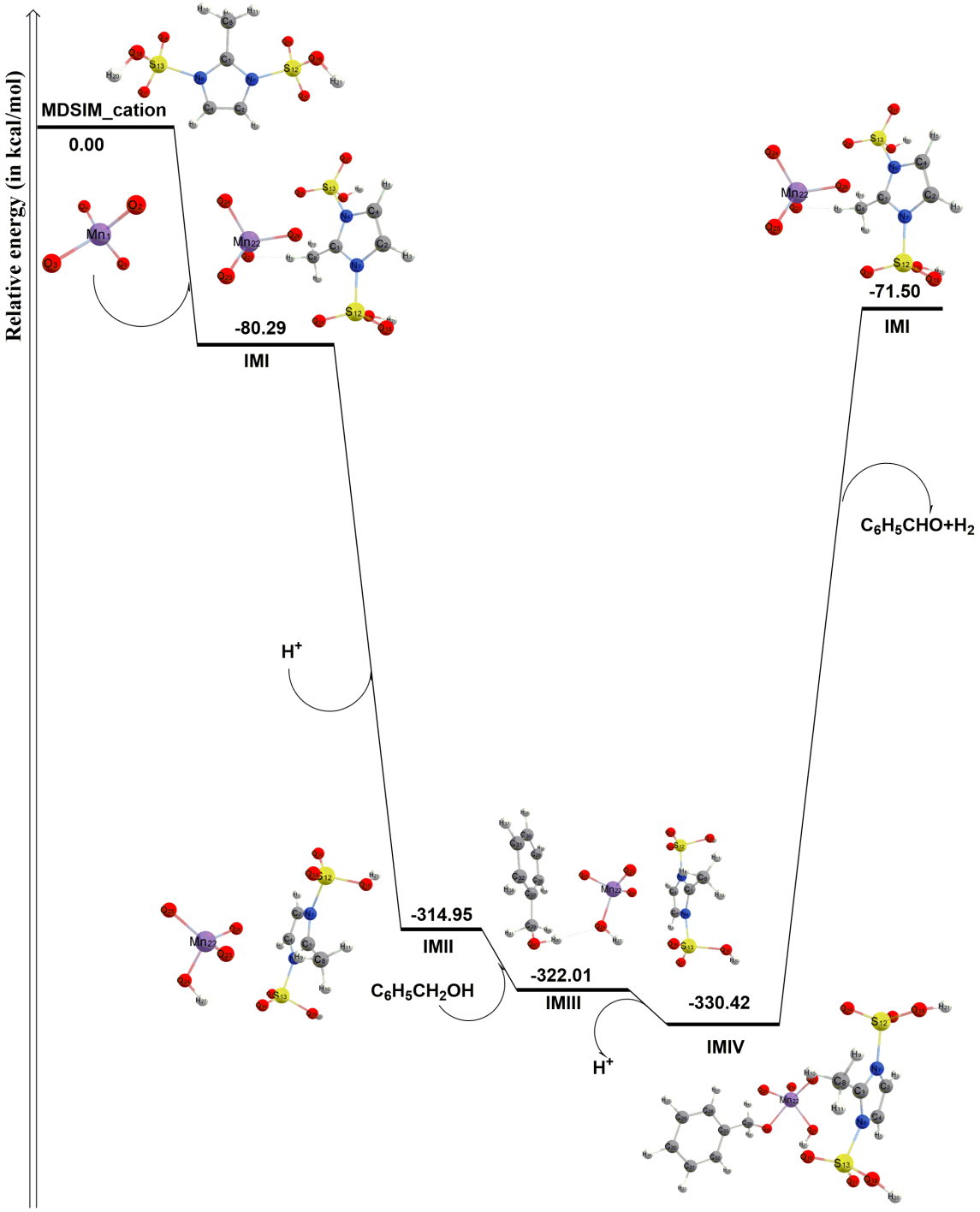

Fig. 3.12: Potential energy diagram of proposed reaction at B3LYP/6-311++G(d,p) level of theory.

It was apparent from **Fig. 3.12** that when MnO_4^- interacted with $[MDSIM]^+$ and formed an intermediate **IM I**, the energy of the **IM I** was decreased by the magnitude of 80.29 kcal/mol relative to $[MDSIM]^+$ cation + MnO_4^- anion, suggesting that **IM I** was stable as compared to $[MDSIM]^+$ cation + MnO_4^- anion. In the next step, as protonation (H^+) took place in **IM I** to form **IM II,** the energy of **IM II** was seen to be further

decreased by the magnitude of 234.66 kcal/mol relative to **IM I**, making it a highly stable intermediate structure in comparison to **IM I**. After that, addition of $C_6H_5CH_2OH$ to **IM II** formed an intermediate **IM III**, which was slightly stable by the magnitude of 7.06 kcal/mol, as compared to **IM II**. Further, intermediate **IM IV** was formed during the deprotonation ($-H^+$) of **IM III**, whose energy was noted to be -8.41 kcal/mol relative to that of **IM III,** signifying this step to be more stable than **IM III** formation step. Lastly, the desorption step would require energy to generate the final products (C_6H_5CHO and H_2) by removing **IM I** ([MDSIM][MnO_4]) completely, making it exothermic as compared to $[MDSIM]^+$ cation + MnO_4^- anion.

3.3. Summary

In summary, an organic-inorganic hybrid material of 2-methyl-1,3-disulfoimidazolium cation in combination with permanganate anion was developed by ion-exchange method at room temperature from a pre-reported room temperature ionic liquid [MDSIM]Cl. Characterization of this material was done by various spectroscopic and analytical techniques like FT-IR, TGA, UV-DRS, PXRD, Raman, SEM, EDX and elemental mapping images. Catalytic amount of the hybrid was employed in the selective oxidation of various substituted primary/secondary aromatic alcohols to carbonyl compounds, in 10% aqueous H_2SO_4 and acetonitrile solution in two methods. **Method A** was conducted under reflux temperature, while **Method B** was done in solvent-drop grinding process at room temperature. Both methods showed controlled oxidation products containing lower to moderate yields depending on the nature of aromatic alcohol. Particularly, the solvent assisted grinding process at room temperature in **Method B** with a short reaction time provided a 'greener' approach to carry out the oxidation reactions. Successful execution of these reactions without the use of any external oxidizing agent also showed that the hybrid possessed oxidizing ability within itself, enabling it to work as a catalyst as well as oxidant in presence of sulfuric acid as co-catalyst. The easy recovery and recyclability of the hybrid catalyst up to three catalytic cycles also added to its suitability in these reactions. Additionally, theoretical calculations were performed for the optimized structure of hybrid and proposed reaction mechanism, as a support to the experimental investigation, which revealed that the reaction scheme, catalysed by the synthesized hybrid, was thermodynamically feasible.

3.4. Experimental data

3.4.1. Synthesis of 2-methyl-1,3-disulfoimidazolium permanganate [MDSIM][MnO_4] hybrid

Preparation of permanganate hybrid of 2-methyl-1,3-disulfoimidazolium cation was carried out *via* formation of 2-methyl-1,3-disulfoimidazolium chloride [MDSIM]Cl as precursor ionic liquid (**Scheme 3.1)** followed by anion-exchange reaction with $KMnO_4$. For that, 10 mmol of 2-methylimidazole in 30 mL dry CH_2Cl_2 was treated with 20 mmol HSO_3Cl at room temperature for 1 h, as stated by the standard procedure, to get 95% yield of [MDSIM]Cl as yellow viscous liquid [28]. The anion exchange reaction of [MDSIM]Cl with MnO_4^- anion was done through treatment with equal equivalent of aqueous $KMnO_4$ solution. For this purpose, 10 mmol of [MDSIM]Cl was added dropwise to an aqueous solution of $KMnO_4$ (10 mmol, in 30 mL distilled water) with continuous stirring at room temperature for 3 h. The resultant brownish black precipitate of product was centrifuged, washed with distilled water for 3-4 times and dried under vacuum at 80 °C for 24 h to produce 93% yield of [MDSIM][MnO_4].

3.4.2. Typical method for oxidation of aromatic alcohol using [MDSIM][MnO_4] as catalyst

For oxidation of aromatic alcohols to aromatic carbonyl compounds, two methods were used (**Scheme 3.2**). In **Method A**, 1 mmol of the alcohol was stirred in a 100 mL two necked round bottom flask using 10 mol% of [MDSIM][MnO_4] catalyst in 6 mL of 10% aqueous sulfuric acid and acetonitrile solution in 1:1 ratio at 80 °C under reflux condition. The reaction mixture was extracted with dichloromethane (3 × 5 mL) after completion of the reaction as monitored by thin layer chromatographic (TLC) technique. The acidic solution of catalyst was then neutralized with 10% aqueous NaOH solution for complete precipitation of the catalyst. The organic extract of CH_2Cl_2 solution was dried over anhydrous sodium sulphate and evaporated under reduced pressure to get the crude product of aromatic carbonyl compound for HPLC analysis.

In **Method B** (**Scheme 3.2**), 1 mmol of the alcohol was grinded using mortar and pestle for an hour at room temperature in presence of 10 mol% of the hybrid catalyst, along with drop-wise addition of 1:1 mixture of 10% sulfuric acid and acetonitrile solution (2 mL). After completion of the reaction, as observed from TLC, the reaction

mixture was diluted with CH_2Cl_2 (6 mL) to dissolve the organic product and then filtered to separate the solid catalyst from the organic extract. The residue of catalyst was washed with more dichloromethane solvent (2 × 3 mL) and then it was reused for next cycle of oxidation reaction. The residue of organic extract, obtained after evaporation of solvent, was subjected for HPLC analysis.

3.4.3. NMR spectra of parent organic salt

a) ^{1}H NMR of [MDSIM]Cl

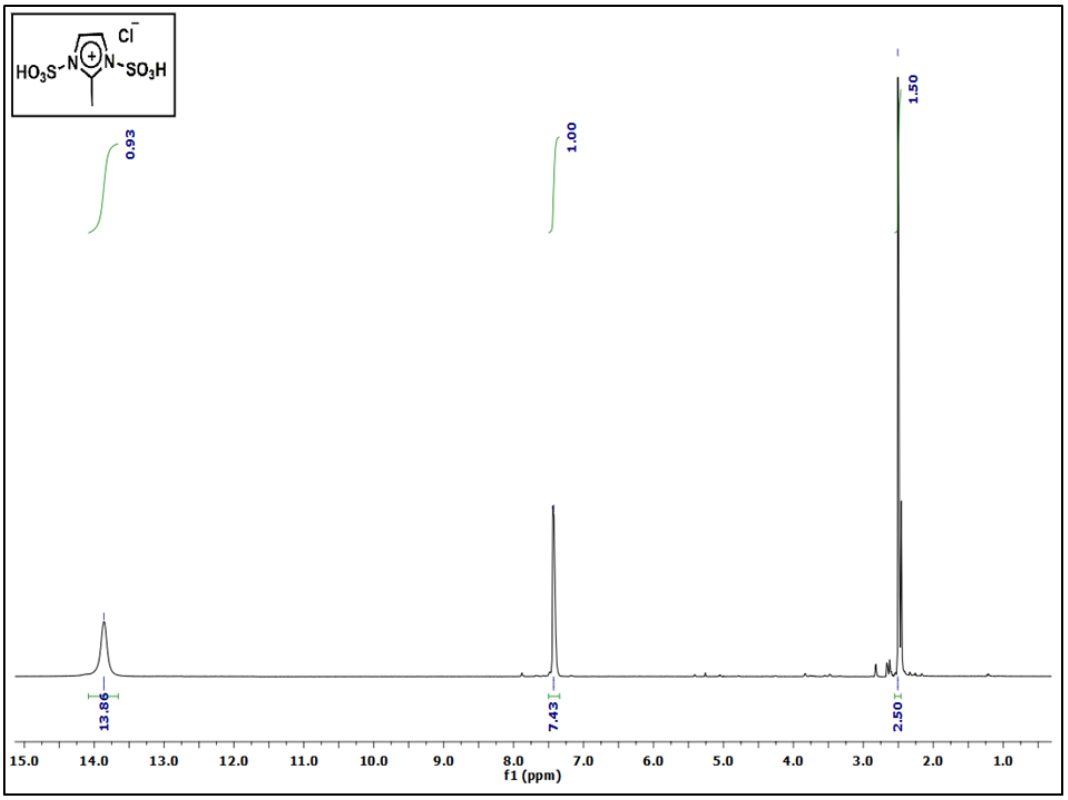

b) ^{13}C NMR of [MDSIM]Cl

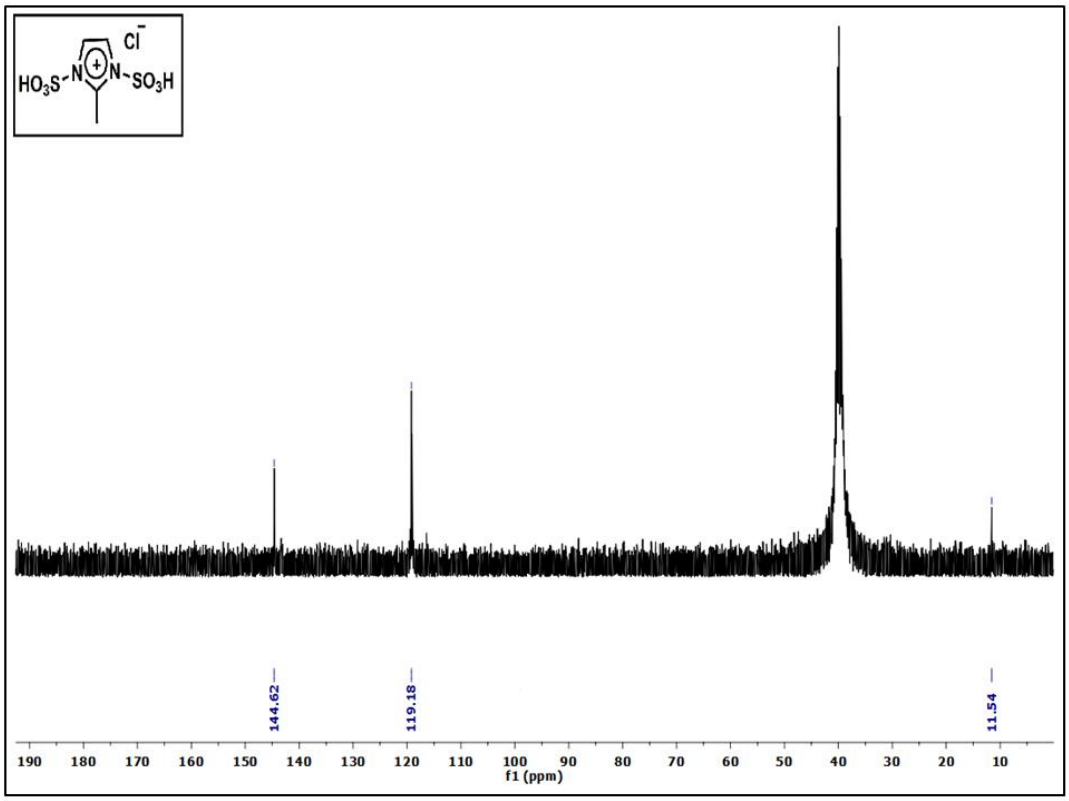

3.4.4. Spectra of solid $KMnO_4$

a) UV-Vis DRS spectrum of $KMnO_4$

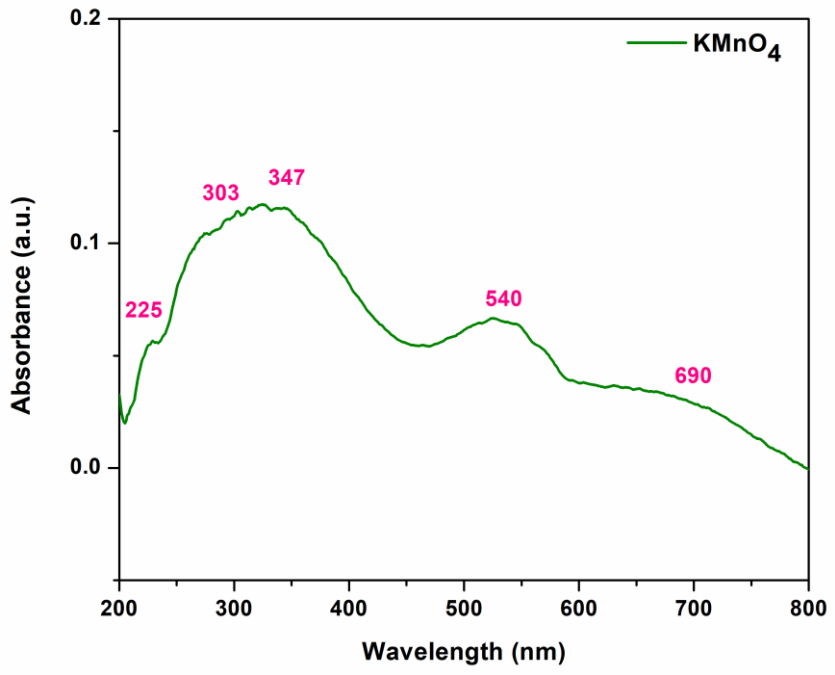

b) Raman spectrum of $KMnO_4$

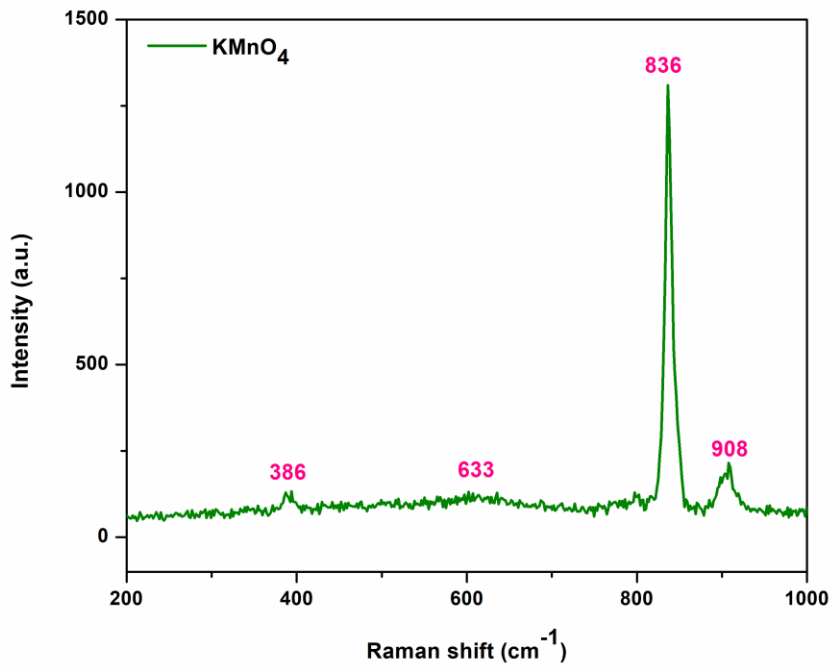

3.4.5. HPLC spectra of oxidized products formed by Method A and Method B

a) HPLC spectra of oxidized products of 4-methoxybenzyl alcohol (4-OMePhCH$_2$OH) (**1a**)

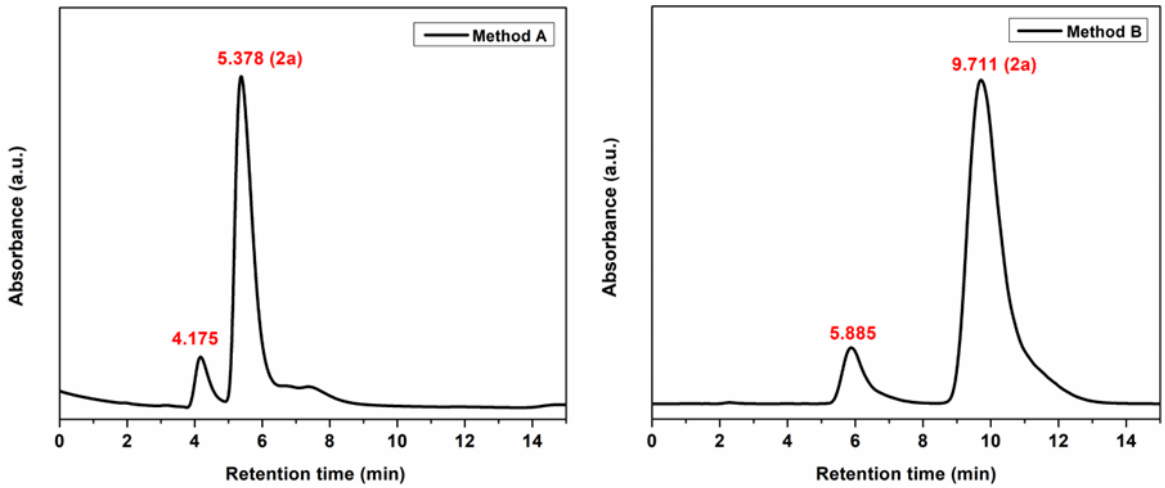

(R.T. 4.175 and 5.885 match the R.T. of 4-OMePhCH$_2$OH, R.T. 5.378 (**2a, Method A**) and 9.711 (**2a, Method B**) match the R.T. of 4-OMePhCHO) *

*Different R.T. because the spectra were recorded on different days

b) HPLC spectra of oxidized products of 4-methylbenzyl alcohol (4-$MePhCH_2OH$) (**1b**)

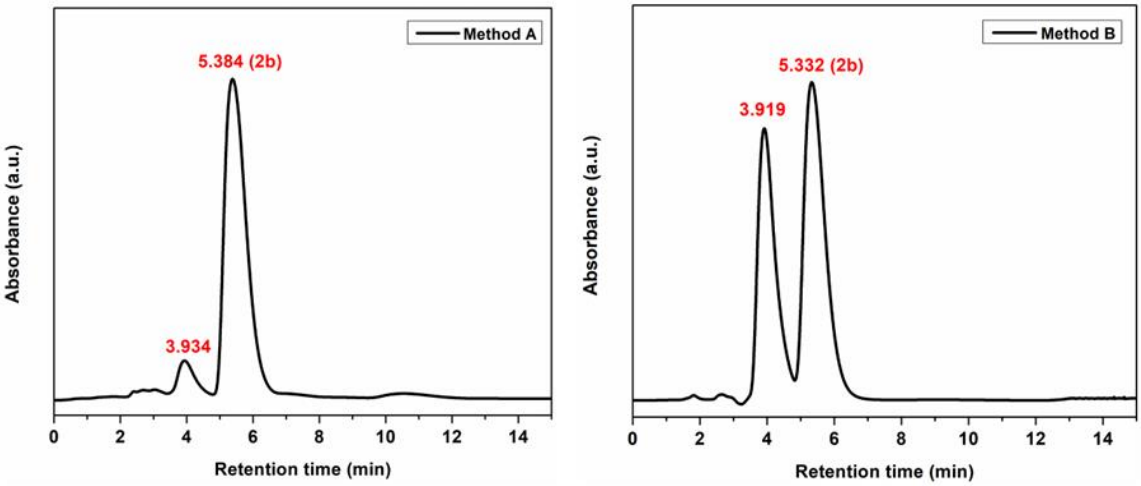

(R.T. 3.934 and 3.919 match the R.T. of 4-$MePhCH_2OH$, R.T. 5.384 (**2b, Method A**) and 5.332 (**2b, Method B**) match the R.T. of 4-MePhCHO)

c) HPLC spectra of oxidized products of 4-nitrobenzyl alcohol (4-NO_2PhCH_2OH) (**1c**)

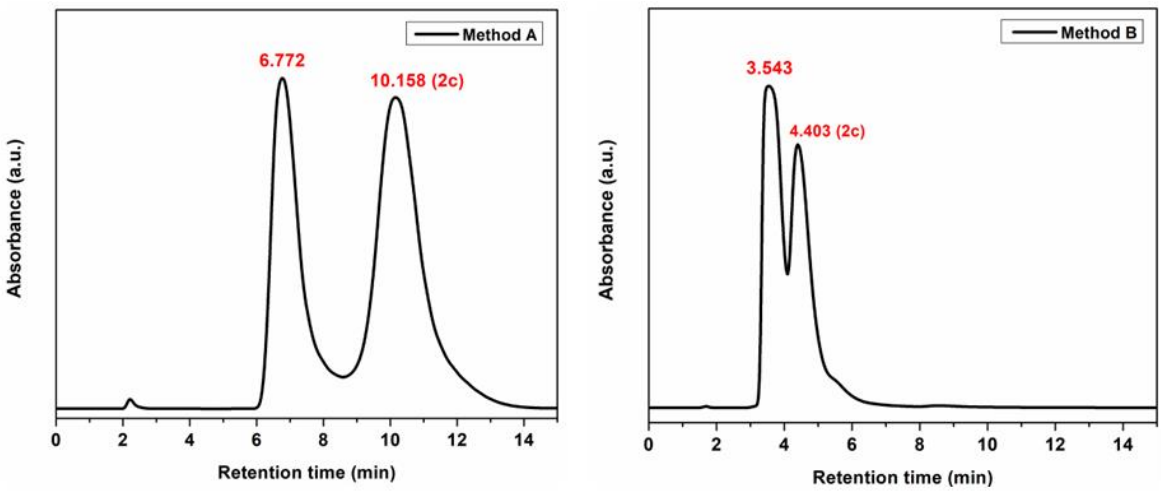

(R.T. 6.772 and 3.543 match the R.T. of 4-NO_2PhCH_2OH, R.T. 10.158 (**2c, Method A**) and 4.403 (**2c, Method B**) match the R.T. of 4-NO_2PhCHO) *

*Different R.T. because the spectra were recorded on different days

d) HPLC spectra of oxidized products of 4-chlorobenzyl alcohol (4-ClPhCH$_2$OH) (**1d**)

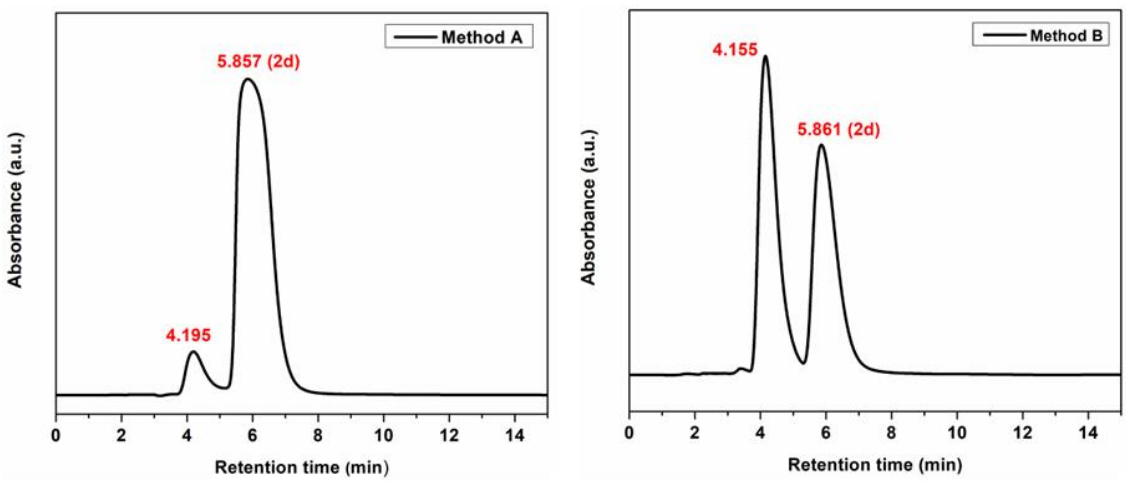

(R.T. 4.195 and 4.155 match the R.T. of 4-ClPhCH$_2$OH, R.T. 5.857 (**2d, Method A**) and 5.861 (**2d, Method B**) match the R.T. of 4-ClPhCHO)

e) HPLC spectra of oxidized products of benzyl alcohol (PhCH$_2$OH) (**1e**)

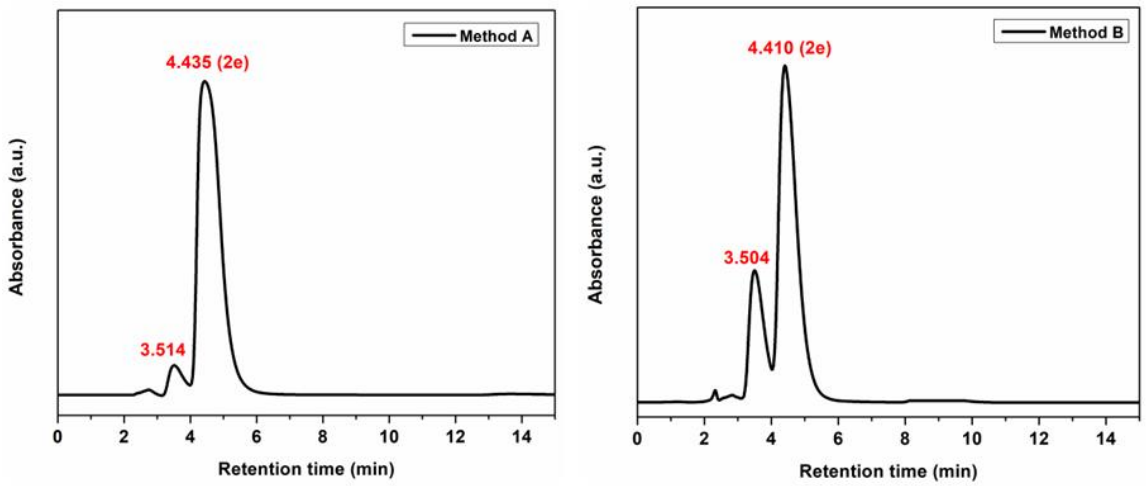

(R.T. 3.514 and 3.504 match the R.T. of PhCH$_2$OH, R.T. 4.435 (**2e, Method A**) and 4.410 (**2e, Method B**) match the R.T. of PhCHO)

f) HPLC spectra of oxidized products of 1-phenylethanol (PhCH(OH)Me) (**1f**)

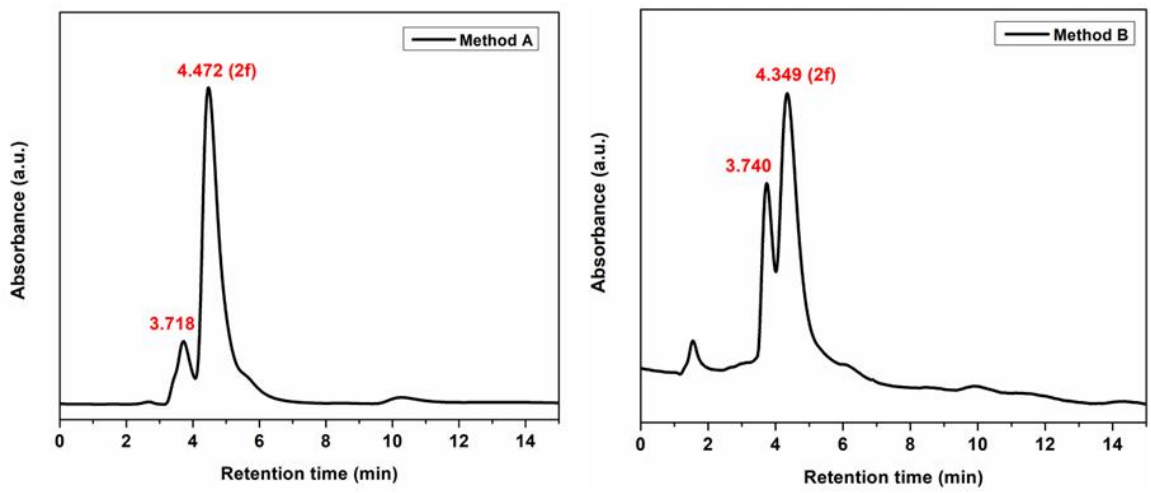

(R.T. 3.718 and 3.740 match the R.T. of PhCH(OH)Me, R.T. 4.472 (**2f, Method A**) and 4.349 (**2f, Method B**) match the R.T. of PhC(O)Me)

g) HPLC spectra of oxidized products of 2-methoxybenzyl alcohol (2-OMePhCH$_2$OH) (**1g**)

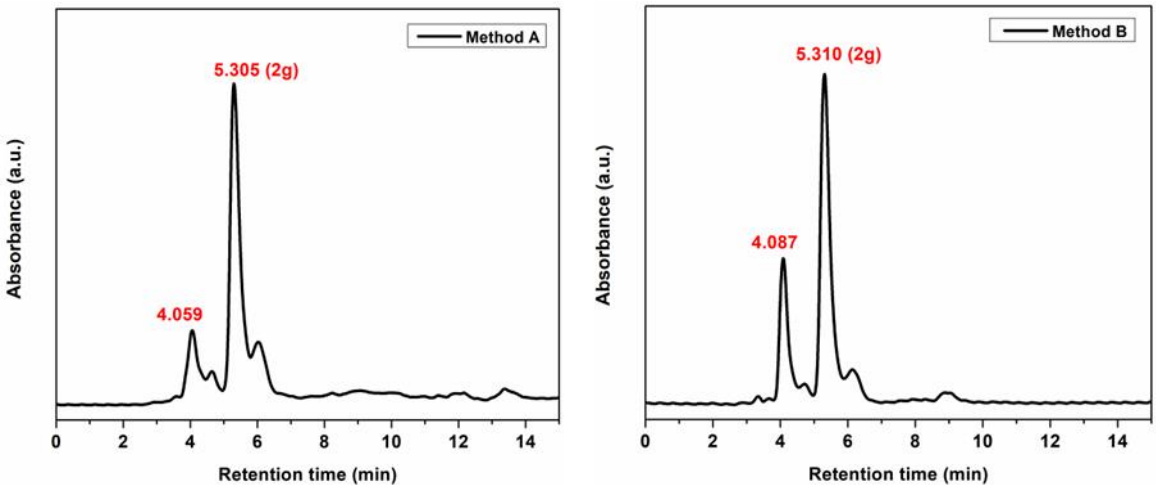

(R.T. 4.059 and 4.087 match the R.T. of 2-OMePhCH$_2$OH, R.T. 5.305 (**2g, Method A**) and 5.310 (**2g, Method B**) match the R.T. of 2-OMePhCHO)

h) HPLC spectra of oxidized products of 3-methoxybenzyl alcohol (3-OMePhCH$_2$OH) (**1h**)

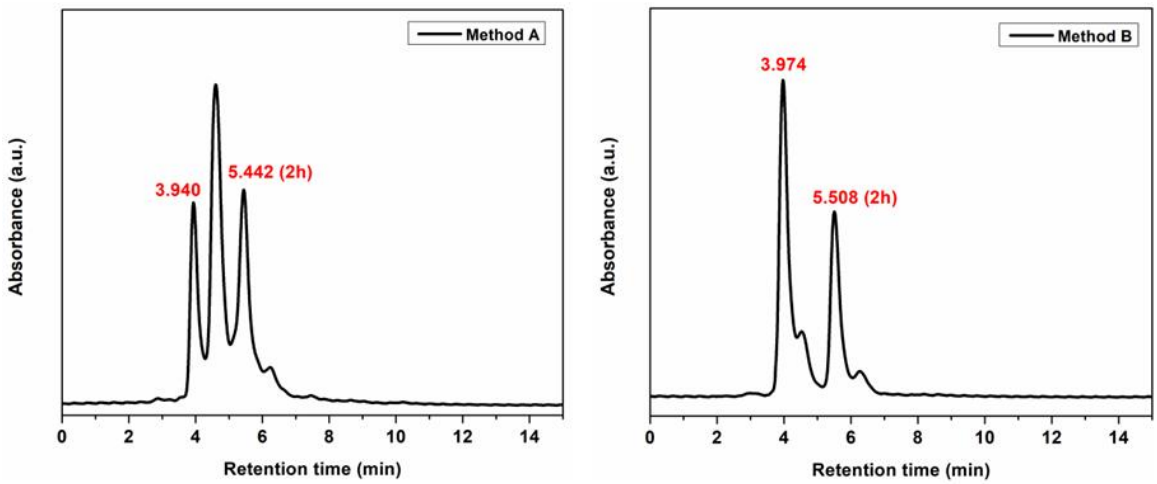

(R.T. 3.940 and 3.974 match the R.T. of 3-OMePhCH$_2$OH, R.T. 5.442 (**2h, Method A**) and 5.508 (**2h, Method B**) match the R.T. of 3-OMePhCHO)

i) HPLC spectra of oxidized products of 4-isopropylbenzyl alcohol (4-(CH$_3$)$_2$CHPhCH$_2$OH) (**1i**)

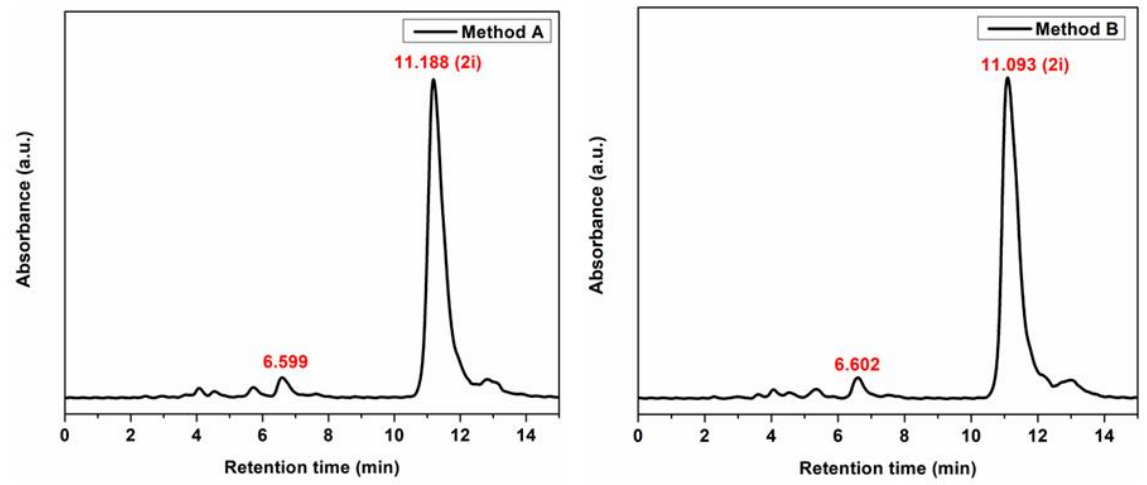

(R.T. 6.599 and 6.602 match the R.T. of 4-(CH$_3$)$_2$CHPhCH$_2$OH, R.T. 11.188 (**2i, Method A**) and 11.093 (**2i, Method B**) match the R.T. of 4-(CH$_3$)$_2$CHPhCHO)

j) HPLC spectra of oxidized products of 2-thiophenemethanol ($C_4H_3SCH_2OH$) (**1j**)

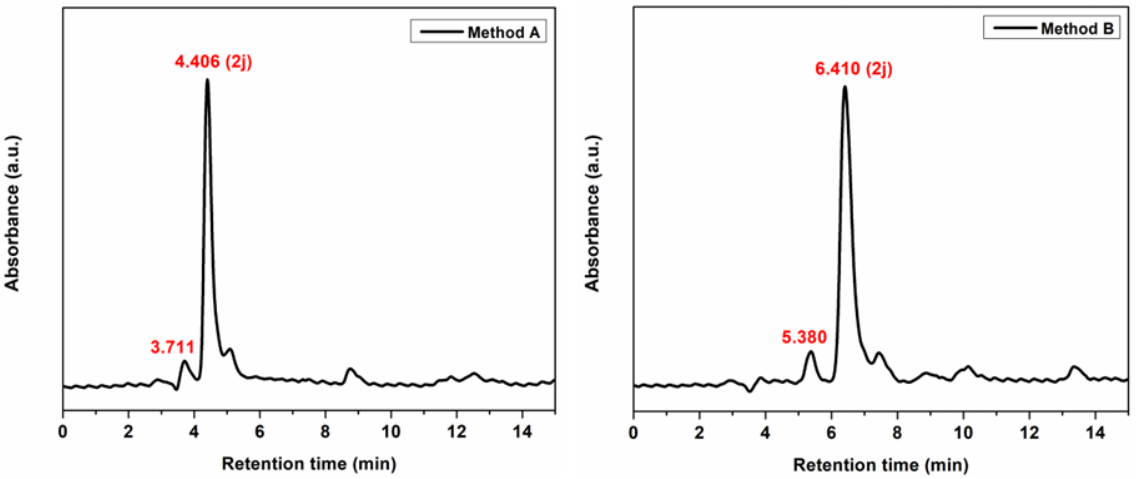

(R.T. 3.711 and 5.380 match the R.T. of $C_4H_3SCH_2OH$, R.T. 4.406 (**2j, Method A**) and 6.410 (**2j, Method B**) match the R.T. of of C_4H_3SCHO) *

*Different R.T. because the spectra were recorded on different days

k) HPLC spectra of oxidized products of biphenyl-4-methanol ($C_6H_5C_6H_4CH_2OH$) (**1k**)

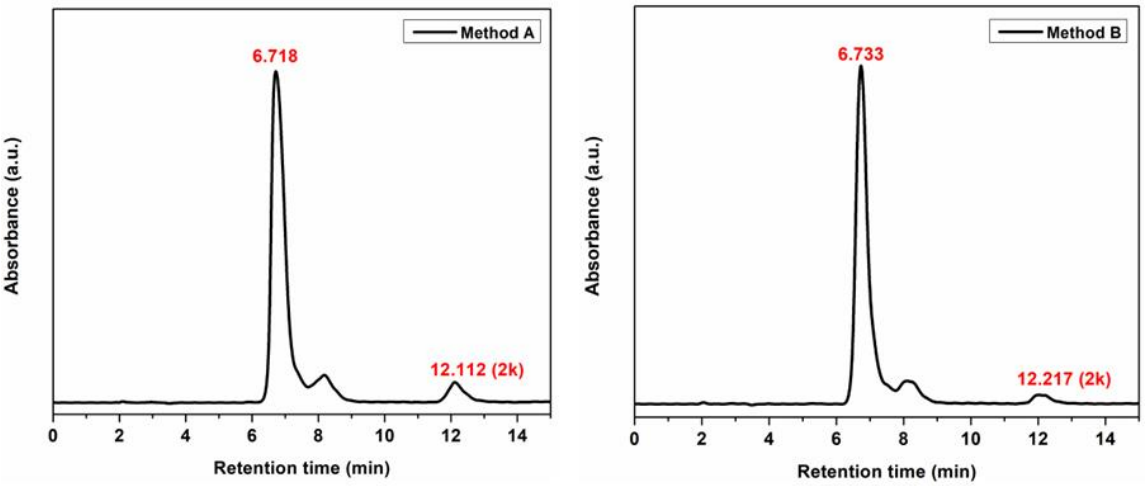

(R.T. 6.718 and 6.733 match the R.T. of $C_6H_5C_6H_4CH_2OH$, R.T. 12.112 (**2k, Method A**) and 12.217 (**2k, Method B**) match the R.T. of $C_6H_5C_6H_4CHO$)

l) HPLC spectra of oxidized products of 1-naphthalenemethanol ($C_{10}H_7CH_2OH$) (**1l**)

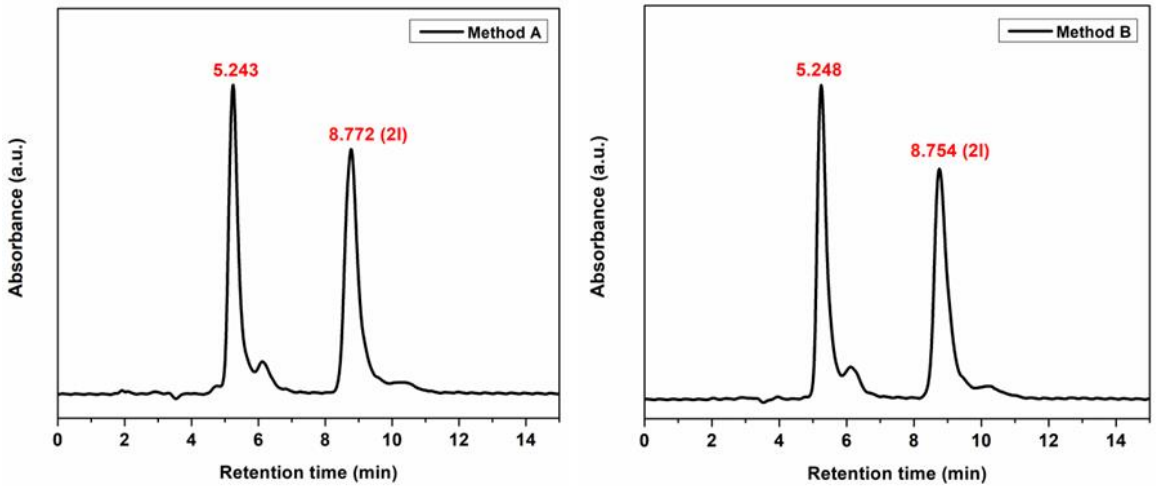

(R.T. 5.243 and 5.248 match the R.T. of $C_{10}H_7CH_2OH$, R.T. 8.772 (**2l, Method A**) and 8.754 (**2l, Method B**) match the R.T. of $C_{10}H_7CHO$)

3.4.6. Theoretical data

Table 3.A: Cartesian coordinates of all species at B3LYP/6-311++G(d,p) level of theory. All values are given in Angstrom.

MDSIM

Z	X	Y	Z
6	-0.000001000	-0.378629000	0.009187000
6	0.674979000	1.776886000	0.007531000
1	1.389377000	2.582449000	0.026519000
6	-0.674970000	1.776891000	0.007566000
1	-1.389363000	2.582457000	0.026587000
7	-1.075906000	0.439350000	0.003577000
7	1.075911000	0.439344000	0.003510000

6	-0.000012000	-1.863031000	0.021164000
1	-0.000143000	-2.227334000	1.053191000
1	-0.886335000	-2.250736000	-0.478719000
1	0.886449000	-2.250752000	-0.478453000
16	2.798026000	-0.057623000	0.122317000
16	-2.798031000	-0.057623000	0.122312000
8	2.816516000	-1.099103000	1.098908000
8	3.500188000	1.192022000	0.186968000
8	-2.816566000	-1.099139000	1.098863000
8	-3.500186000	1.192024000	0.186977000
8	-2.971323000	-0.738634000	-1.316717000
8	2.971355000	-0.738671000	-1.316691000
1	-3.415302000	-0.141797000	-1.946014000
1	3.415516000	-0.141911000	-1.945932000

MnO_4

Z	**X**	**Y**	**Z**
25	-0.000024000	0.000003000	0.011382000
8	-0.002744000	-0.001042000	1.599986000
8	0.747906000	1.380696000	-0.543154000
8	0.822982000	-1.336668000	-0.544674000

8	-1.568070000	-0.042995000	-0.547728000

MDSIM_MnO_4

Z	X	Y	Z
6	-3.627182000	1.060176000	-1.173352000
6	-4.841282000	0.845403000	0.714383000
1	-5.346501000	1.178198000	1.603786000
6	-4.706075000	-0.375673000	0.150225000
1	-5.068679000	-1.342478000	0.451916000
7	-3.959329000	-0.220644000	-1.006929000
7	-4.168781000	1.740656000	-0.119685000
6	-2.834334000	1.626616000	-2.296083000
1	-1.851798000	1.948815000	-1.943629000
1	-2.719430000	0.870795000	-3.069521000
1	-3.340310000	2.497532000	-2.711808000
16	-3.851559000	3.410147000	0.366332000
16	-3.298945000	-1.714020000	-1.997840000
8	-4.966843000	3.762534000	1.198559000
8	-3.500817000	4.105702000	-0.845476000
8	-4.092675000	-2.765922000	-1.391860000
8	-3.549883000	-1.314134000	-3.369091000

8	-1.876870000	-1.653792000	-1.579489000
8	-2.607670000	3.206566000	1.314504000
1	-1.771273000	2.927540000	0.833838000
1	-1.207476000	-2.219524000	-0.167529000
25	-1.497606000	-2.817384000	2.083174000
8	-2.760936000	-1.902356000	2.242674000
8	-0.647051000	-2.344704000	0.650197000
8	-0.486346000	-2.612190000	3.260476000
8	-1.931833000	-4.313635000	1.968610000
6	1.539762000	-0.280869000	-0.505227000
6	1.882965000	-0.091688000	1.700501000
1	1.851238000	0.399117000	2.657075000
6	2.361380000	-1.299145000	1.329547000
1	2.821294000	-2.094124000	1.888509000
7	2.147797000	-1.401909000	-0.043571000
7	1.385758000	0.523263000	0.557509000
16	0.920101000	2.315099000	0.539275000
16	2.763568000	-2.753948000	-1.008710000
8	1.131847000	2.667910000	1.926670000
8	-0.477147000	2.284623000	0.062506000

8	3.445933000	-3.565629000	-0.036155000
8	1.708497000	-3.218607000	-1.858117000
8	3.784000000	-1.964480000	-1.947199000
8	1.863093000	2.832380000	-0.463216000
1	4.428746000	-1.421233000	-1.432732000
25	5.373232000	1.484840000	-0.017552000
8	4.977798000	0.041369000	-0.554044000
8	4.505228000	2.679288000	-0.893067000
8	4.996748000	1.594337000	1.491954000
8	6.883855000	1.772711000	-0.248653000
6	1.101608000	-0.025045000	-1.899187000
1	1.802938000	-0.459419000	-2.610750000
1	0.121763000	-0.489313000	-2.057172000
1	1.028517000	1.045882000	-2.077114000
1	3.539072000	2.771369000	-0.664705000

IM I

Z	**X**	**Y**	**Z**
6	0.000689000	0.973485000	0.403012000
6	-0.670344000	1.756003000	-1.615757000
1	-1.384127000	1.985975000	-2.386096000

6	0.672592000	1.755183000	-1.615792000
1	1.386611000	1.984298000	-2.386168000
7	1.078205000	1.317870000	-0.348146000
7	-1.076435000	1.319190000	-0.348093000
6	0.000427000	0.466052000	1.784942000
1	-0.000311000	-0.645378000	1.761715000
1	0.891188000	0.792045000	2.318885000
1	-0.889828000	0.793245000	2.318996000
16	-2.766807000	1.105724000	0.075248000
16	2.768334000	1.102491000	0.075195000
8	-2.880023000	-0.080734000	0.857812000
8	-3.467029000	1.395548000	-1.149609000
8	2.880261000	-0.084266000	0.857493000
8	3.468894000	1.391821000	-1.149587000
8	2.949643000	2.347725000	1.096515000
8	-2.946796000	2.351384000	1.096291000
1	3.260325000	3.131870000	0.614909000
1	-3.256706000	3.135732000	0.614521000
25	-0.001830000	-2.703040000	-0.127341000
8	-0.001429000	-2.513516000	1.469690000

8	1.294301000	-3.489177000	-0.580259000
8	-1.299227000	-3.487343000	-0.579816000
8	-0.000896000	-1.218563000	-0.786664000

IM II

Z	**X**	**Y**	**Z**
6	-0.901731000	0.853097000	0.414308000
6	-1.760972000	0.890424000	-1.673258000
1	-2.434935000	0.603351000	-2.462331000
6	-0.697944000	1.719843000	-1.664331000
1	-0.247285000	2.312664000	-2.441705000
7	-0.186235000	1.699329000	-0.362946000
7	-1.879816000	0.374437000	-0.381624000
6	-0.668262000	0.527303000	1.842101000
1	-0.081208000	-0.393858000	1.921691000
1	-0.125821000	1.331152000	2.336518000
1	-1.616186000	0.373166000	2.357463000
16	-3.075826000	-0.891351000	0.047869000
16	1.350335000	2.490228000	0.060084000
8	-2.348241000	-1.849898000	0.816249000
8	-3.767821000	-1.126975000	-1.187076000

8	2.151720000	1.476962000	0.680871000
8	1.695543000	3.224715000	-1.122671000
8	0.850172000	3.463291000	1.226413000
8	-3.988091000	-0.050938000	1.063000000
1	0.676725000	4.363118000	0.894628000
1	-4.799019000	0.272569000	0.630835000
25	1.975043000	-2.013062000	-0.087085000
8	1.629711000	-2.101047000	1.436245000
8	3.519910000	-1.234014000	-0.276108000
8	2.126301000	-3.418517000	-0.725569000
8	0.870750000	-1.158260000	-0.820676000
1	3.575690000	-0.380573000	0.186436000

IM III

Z	**X**	**Y**	**Z**
6	-2.817137000	-0.056473000	0.286130000
6	-3.001465000	-0.716838000	-1.865675000
1	-3.062560000	-1.427489000	-2.671786000
6	-2.950790000	0.629792000	-1.864349000
1	-2.960449000	1.346197000	-2.667411000
7	-2.856530000	1.025176000	-0.526364000

7	-2.933117000	-1.123452000	-0.531606000
6	-2.685395000	-0.067358000	1.761879000
1	-1.629663000	-0.184728000	2.033833000
1	-3.055025000	0.863975000	2.187471000
1	-3.245189000	-0.898532000	2.189702000
16	-2.840665000	-2.843620000	-0.052107000
16	-2.563057000	2.715149000	-0.061586000
8	-1.820818000	-2.911772000	0.944390000
8	-2.861916000	-3.540972000	-1.307134000
8	-1.414767000	2.699280000	0.794392000
8	-2.679214000	3.435068000	-1.297827000
8	-3.835970000	2.968249000	0.876297000
8	-4.253344000	-2.981304000	0.696602000
1	-4.560204000	3.398207000	0.386735000
1	-4.926755000	-3.375903000	0.114304000
25	1.154424000	0.221519000	0.503611000
8	0.682995000	-0.077630000	1.971426000
8	1.673999000	1.909625000	0.392185000
8	2.467763000	-0.564682000	0.141360000
8	-0.002390000	-0.040389000	-0.545787000

1	0.986945000	2.528581000	0.683679000
6	4.845637000	-0.853579000	-1.516871000
6	5.009589000	-2.156355000	-1.076006000
6	5.229679000	-2.415285000	0.285459000
6	5.291099000	-1.361698000	1.197043000
6	5.124190000	-0.053278000	0.758392000
6	4.892834000	0.220024000	-0.606806000
1	4.674759000	-0.653533000	-2.569657000
1	4.968311000	-2.978120000	-1.781414000
1	5.359275000	-3.436142000	0.625871000
1	5.469798000	-1.561633000	2.246945000
1	5.179097000	0.777125000	1.451760000
6	4.809271000	1.644717000	-1.108166000
1	3.487380000	2.430206000	0.092326000
1	5.808407000	1.952138000	-1.440058000
1	4.162584000	1.681260000	-1.996032000
8	4.416749000	2.587261000	-0.135636000

IM IV

Z	**X**	**Y**	**Z**
6	2.530655000	0.632939000	-0.600324000

6	3.188208000	-0.072778000	1.440114000
1	3.666806000	-0.732972000	2.142096000
6	2.412587000	1.015041000	1.620583000
1	2.064905000	1.505523000	2.512096000
7	2.031730000	1.449583000	0.351611000
7	3.264220000	-0.287163000	0.061826000
6	2.311416000	0.719295000	-2.064054000
1	3.191764000	0.379681000	-2.607769000
1	1.469250000	0.074670000	-2.333785000
1	2.078965000	1.739507000	-2.361540000
16	4.093586000	-1.692397000	-0.646057000
16	0.952221000	2.841855000	0.095946000
8	3.267792000	-2.147110000	-1.718302000
8	4.509344000	-2.453536000	0.499016000
8	-0.011320000	2.442307000	-0.879281000
8	0.692207000	3.337331000	1.418455000
8	1.992268000	3.816763000	-0.657677000
8	5.355582000	-0.946385000	-1.307701000
1	2.396762000	4.442926000	-0.032500000
1	6.134482000	-0.991799000	-0.726048000

25	-1.056038000	-1.076932000	0.895438000
8	0.519414000	-1.241030000	0.286716000
8	-0.608481000	0.500303000	1.636159000
8	-1.535427000	-1.237660000	-0.681693000
8	-1.297932000	-2.296819000	1.837570000
1	-1.406684000	0.879327000	2.035664000
6	-4.540588000	-1.317055000	-1.082002000
6	-5.156833000	-0.851927000	-2.232465000
6	-5.935492000	0.310561000	-2.187134000
6	-6.104182000	1.010993000	-0.984875000
6	-5.495262000	0.551440000	0.169727000
6	-4.749179000	-0.645126000	0.139833000
1	-3.927990000	-2.209280000	-1.108654000
1	-5.034357000	-1.386759000	-3.166377000
1	-6.406359000	0.677079000	-3.092030000
1	-6.709464000	1.908976000	-0.960758000
1	-5.612286000	1.086036000	1.105192000
6	-4.124839000	-1.172824000	1.420356000
8	-2.969456000	-0.384821000	1.391826000
1	-4.727420000	-0.932886000	2.300368000

1	-3.912873000	-2.243095000	1.376562000

$C_6H_5CH_2OH$

Z	X	Y	Z
6	0.418114000	1.278309000	0.017866000
6	1.788284000	1.070006000	-0.145335000
6	2.301871000	-0.224223000	-0.134266000
6	1.440069000	-1.308486000	0.041163000
6	0.074889000	-1.097366000	0.210250000
6	-0.451729000	0.200436000	0.199938000
1	0.022045000	2.289073000	0.001850000
1	2.450320000	1.917240000	-0.286003000
1	3.365506000	-0.389629000	-0.264141000
1	1.834955000	-2.318460000	0.051306000
1	-0.595277000	-1.939698000	0.342674000
6	-1.935408000	0.425839000	0.395554000
1	-2.487302000	-0.217361000	-1.369856000
1	-2.234693000	0.148484000	1.409805000
1	-2.167967000	1.490377000	0.264936000
8	-2.750516000	-0.380891000	-0.457698000

C_6H_5CHO

Z	X	Y	Z
6	-0.038080000	-1.104744000	0.000000000
6	1.332750000	-1.325887000	0.000000000
6	2.216615000	-0.242362000	0.000000000
6	1.729429000	1.063830000	0.000000000
6	0.354869000	1.286754000	0.000000000
6	-0.533834000	0.206308000	0.000000000
1	-0.742508000	-1.928281000	0.000000000
1	1.719475000	-2.338640000	0.000000000
1	3.286483000	-0.419163000	0.000000000
1	2.417471000	1.901326000	0.000000000
1	-0.034927000	2.300149000	0.000000000
6	-1.992405000	0.463574000	0.000000000
1	-2.270908000	1.538757000	0.000000000
8	-2.848893000	-0.392373000	0.000000000

H_2

Z	X	Y	Z
1	0.000000000	0.000000000	0.372064000
1	0.000000000	0.000000000	-0.372064000

Table 3.B: Vibrational frequency of all species obtained at B3LYP/6-311++G(d,p) level of theory.

Species	**Frequencies (in cm^{-1})**									
MDSIM_MnO_4 : 6	11	16	17	21	24	24	28	29	33	
37	41	49	53	63	65	71	82	83	94	
109	115	122	127	135	142	151	155	162	175	
189	212	217	223	231	246	295	300	317	318	
320	327	328	332	335	335	339	349	352	364	
386	388	399	403	409	412	447	459	484	498	
509	515	519	520	544	551	554	563	574	586	
594	620	628	669	674	697	701	709	718	753	
754	763	773	778	819	861	886	889	954	956	
980	991	1002	1008	1021	1025	1028	1039	1045	1051	
1058	1060	1066	1072	1093	1118	1159	1164	1180	1180	
1183	1185	1195	1198	1202	1214	1216	1287	1301	1320	
1336	1336	1406	1414	1415	1422	1433	1435	1483	1485	
1489	1499	1518	1527	1587	1587	3034	3061	3097	3120	
3127	3160	3164	3179	3233	3286	3291	3304	3308	3422	
MDSIM_cation: 30	51	52	54	117	128	206	210	225	269	
275	315	319	338	359	369	428	451	489	495	
537	562	571	614	668	693	760	804	816	898	
956	1019	1051	1061	1120	1120	1169	1176	1181	1184	
1200	1326	1409	1422	1438	1446	1487	1488	1504	1589	
3051	3126	3159	3277	3294	3706	3707				
MnO_4^- :	366	366	415	415	425	768	791	791	980	
IM I:	18	25	30	34	42	50	79	106	129	149
151	196	228	231	248	276	277	323	325	342	
363	363	375	385	412	414	424	432	454	490	
491	543	573	585	607	625	701	729	773	786	
876	912	930	953	991	1013	1030	1039	1057	1130	
1131	1166	1167	1181	1182	1196	1310	1406	1420	1429	

	1442	1483	1483	1510	1610	2799	3106	3161	3292	3310
	3744	3745								
IM II:	25	30	32	40	44	56	59	64	87	114
	120	143	207	217	230	270	271	279	306	315
	325	339	359	361	375	381	403	415	429	453
	489	496	540	567	573	616	666	694	735	755
	804	818	871	894	955	998	1021	1037	1050	1061
	1080	1123	1125	1169	1174	1180	1185	1200	1324	1409
	1421	1428	1444	1484	1493	1508	1593	3041	3120	3158
	3280	3298	3705	3711	3735					
IM III:	11	13	16	29	30	36	40	49	54	60
	61	76	85	104	116	121	136	146	162	193
	209	219	233	236	271	275	281	316	317	326
	339	362	370	377	388	390	396	401	410	430
	447	453	490	497	541	551	569	574	598	616
	616	664	673	695	697	744	752	797	801	815
	853	893	916	930	955	956	985	1000	1008	1011
	1013	1023	1029	1038	1051	1062	1074	1115	1124	1125
	1170	1173	1180	1183	1186	1192	1201	1217	1229	1316
	1324	1362	1395	1411	1422	1425	1428	1443	1474	1477
	1486	1493	1509	1509	1573	1596	1624	2986	3024	3031
	3116	3157	3164	3176	3185	3194	3201	3282	3300	3688
	3709	3714	3765							
IM IV :	6	10	21	27	30	36	43	50	60	65
	72	80	85	106	122	133	146	162	178	213
	217	233	271	274	277	281	314	319	327	337
	340	345	350	362	372	374	376	400	430	454
	482	487	494	538	542	570	573	573	576	611
	615	657	669	674	697	745	771	788	801	802
	834	846	885	948	957	958	983	996	1000	1004
	1013	1019	1023	1037	1046	1062	1118	1126	1127	1168
	1171	1182	1185	1187	1188	1203	1212	1216	1320	1329

	1353	1360	1413	1417	1436	1444	1473	1486	1492	1493
	1512	1513	1570	1595	1605	3041	3053	3103	3128	3165
	3179	3185	3193	3200	3206	3288	3308	3721	3725	3750
$C_6H_5CH_2OH$:	30	153	270	325	399	411	481	603	634	702
	751	816	859	921	977	981	991	1017	1032	1050
	1107	1182	1196	1200	1224	1319	1350	1373	1412	1483
	1503	1526	1624	1644	3002	3068	3155	3163	3173	3181
	3189	3821								
C_6H_5CHO:	117	219	234	415	442	463	630	661	702	763
	836	864	941	995	1011	1016	1033	1043	1101	1184
	1188	1222	1334	1352	1417	1484	1520	1622	1638	1768
	2888	3157	3167	3178	3188	3195				
H_2:	4418									

Table 3.C: Total energy, Enthalpy and Gibb's free energy of all species obtained at B3LYP/6-311++G(d,p) level of theory. All values are in Hartree.

Species	E_0	H	G
MDSIM	-1513.567208	-1513.551699	-1513.61029
MnO_4^-	-1452.005407	-1451.999776	-1452.033818
IM I	-2965.700562	-2965.678931	-2965.753679
IM II	-2966.074525	-2966.051805	-2966.12896
IM III	-3312.829136	-3312.797694	-3312.897275
IM IV	-3312.842541	-3312.810987	-3312.915465
H^+	0.000000	0.002360	-0.010000
H_2	-1.169506	-1.166201	-1.180996
$C_6H_5CH_2OH$	-346.743372	-346.73533	-346.775582
C_6H_5CHO	-345.559857	-345.552577	-345.590448

3.5. Bibliography

[1] Zhang, W. H., Shen, J. J., Wu, J., Liang, X. Y., Xu, J., Liu, P., Xue, B., and Li, Y. X. An amphiphilic graphene oxide-immobilized polyoxometalate-based ionic

liquid: A highly efficient triphase transfer catalyst for the selective oxidation of alcohols with aqueous H_2O_2. *Molecular Catalysis*, 443:262-269, 2017.

[2] Rajabi, F., Nafe, M., Bardajee, G. R., and Luque, R. Tungstate ion (WO_4^{2-}) confined in hydrophilic/hydrophobic nanomaterials functionalized brönsted acidic ionic liquid as highly active catalyst in the selective aerobic oxidation of alcohols in water. *Molecular Catalysis*, 497:111202, 2020.

[3] Rahman, M. and Rocek, J. Chromium (IV) oxidation of primary and secondary alcohols. *Journal of the American Chemical Society*, 93(21):5455-5462, 1971.

[4] Lee, D. G. and Chen, T. The oxidation of alcohols by permanganate. A comparison with other high-valent transition-metal oxidants. *The Journal of Organic Chemistry*, 56(18):5341-5345, 1991.

[5] Fieser, M. and Fieser, L. F. *Reagents for Organic Synthesis* (Vol. 1). John Wiley & Sons, New York, 1974.

[6] Evans, W. L. and Day, J. E. The oxidation of ethyl alcohol by means of potassium permanganate. *Journal of the American Chemical Society*, 41(8):1267-1285, 1919.

[7] Chandrasekaran, S. Substituent-directed oxidative cyclization. Application to the synthesis of natural products. *ChemInform*, 21(4), 1990.

[8] Nakamura, K., Nishiyama, S., Tsuruya, S., and Masai, M. Oxidation of catechol with $KMnO_4$ by using crown ethers as phase transfer catalysts. *Journal of Molecular Catalysis*, 93(2):195-210, 1994.

[9] Jose, N., Sengupta, S., and Basu, J. K. Selective production of benzaldehyde by permanganate oxidation of benzyl alcohol using 18-crown-6 as phase transfer catalyst. *Journal of Molecular Catalysis A: Chemical*, 309(1-2):153-158, 2009.

[10] Herriott, A. W. and Picker, D. Purple benzene: Permanganate oxidations using quaternary ammonium ions. *Tetrahedron Letters*, 15(16):1511-1514, 1974.

[11] Shaabani, A. and Lee, D. G. Solvent free permanganate oxidations. *Tetrahedron Letters*, 42(34):5833-5836, 2001.

[12] Shaabani, A., Mirzaei, P., Naderi, S., and Lee, D. G. Green oxidations. The use of potassium permanganate supported on manganese dioxide. *Tetrahedron*, 60(50):11415-11420, 2004.

[13] Shaabani, A., Bazgir, A., and Lee, D. G. Oxidation of organic compounds by potassium permanganate supported on montmorillonite K10. *Synthetic Communications*, 34(19):3595-3607, 2004.

[14] Firouzabadi, H., Fakoorpour, M., and Hazarkhani, H. Highly selective oxidation of primary and secondary benzylic alcohols by $KMnO_4/ZrOCl_2 \cdot 8H_2O$ in diethyl ether. *Synthetic Communications*, 31(24):3859-3862, 2001.

[15] Lou, J. D., Wang, G. Q., Li, L., and Zhu, L. Y. Oxidation of alcohols catalyzed by a new potassium permanganate adsorbed on graphite reagent. *Synthesis and Reactivity in Inorganic, Metal-Organic and Nano-Metal Chemistry*, 35(4):281-283, 2005.

[16] Lou, J. D., Pan, L. L., Li, L., Li, F., and Gao, C. L. Selective oxidation of alcohols with potassium permanganate adsorbed on silica gel under solvent-free conditions. *Synthesis and Reactivity in Inorganic and Metal-Organic Chemistry*, 36(10):729-731, 2006.

[17] Lou, J. D., Zhu, L. Y., and Wang, L. Z. Efficient oxidation of alcohols with potassium permanganate adsorbed on aluminum silicate reagent. *Monatshefte für Chemie*, 135:31-34, 2004.

[18] Lou, J. D. and Lou, W. X. Oxidation of alcohols to carbonyl compounds with a new potassium permanganate adsorbed on Kieselguhr reagent. *Synthetic Communications*, 27(21):3697-3699, 1997.

[19] Kumar, A., Jain, N., and Chauhan, S. M. S. Oxidation of benzylic alcohols to carbonyl compounds with potassium permanganate in ionic liquids. *Synthetic Communications*, 34(15):2835-2842, 2004.

[20] Safaei-Ghomi, J., Emaeili, M., and Adbol, R. Mild and efficient method for oxidation of alcohols in ionic liquid media. *Digest Journal of Nanomaterials and Biostructures*, 5(4):865-871, 2010.

[21] Jasim, S. A., Abdulkadhim, A. H., Yasin, G., Abdelbasset, W. K., Jawad, M. A., and Kazemnejadi, M. Gram scale, metal-free and selective aerobic oxidation of alcohol and alkyl benzenes using homogeneous recyclable TAIm $[MnO_4]$ oxidative ionic liquid under mild conditions: Microwave/ultrasonic-assisted to carboxylic acid. *Journal of Saudi Chemical Society*, 26(4):101487, 2022.

[22] Acharjee, A., Ali, M. A., and Saha, B. A review of the synthesis and utility of some lipopathic permanganate oxidants. *Journal of Solution Chemistry*, 47:1449-1478, 2018.

[23] Bhushan, V., Rathore, R., and Chandrasekaran, S. A simple and mild method for the cis hydroxylation of alkenes with cetyltrimethylammonium permanganate. *Synthesis*, 1984(05):431-433, 1984.

[24] Vimala, B. C. and Nagendrappa, G. Solvent-free reactions using cetyltrimethylammonium permanganate and cetyltrimethylammonium dichromate-cis-1, 2-dihydroxylation of alkenes, oxidation of alcohols and regeneration of aldehydes and ketones from oximes. *Journal of Saudi Chemical Society*, 13(2):169-175, 2009.

[25] Garnayak, S. and Patel, S. Oxidation of carbamazepine by lipopathic Mn(VII), cetyltrimethylammonium permanganate: A mechanistic study. *International Journal of Chemical Kinetics*, 47(7):429-438, 2015.

[26] Sankhla, R., Kothari, S., Kótai, L., and Banerji, K. K. Kinetics and mechanism of the oxidative regeneration of carbonyl compounds from oximes by cetyltrimethylammonium permanganate. *Journal of Chemical Research*, 2001(4):127-128, 2001.

[27] Sala, T. and Sargent, M. V. Tetrabutylammonium permanganate: An efficient oxidant for organic substrates. *Journal of the Chemical Society, Chemical Communications*, (6):253-254, 1978.

[28] Karaman, H., Barton, R. J., Robertson, B. E., and Lee, D. G. Preparation and properties of quaternary ammonium and phosphonium permanganates. *The Journal of Organic Chemistry*, 49(23):4509-4516, 1984.

[29] Schmidt, H. J. and Schäfer, H. J. Stability of benzyl (triethyl) ammonium permanganate. *Angewandte Chemie International Edition in English*, 18(10):787-787, 1979.

[30] Kashyap, N., Das, S., and Borah, R. Solvent responsive self-separation behaviour of Brønsted acidic ionic liquid-polyoxometalate hybrid catalysts on H_2O_2 mediated oxidation of alcohols. *Polyhedron*, 196:114993, 2021.

[31] Saikia, S. and Borah, R. 2-Methyl-1, 3-disulfoimidazolium polyoxometalate hybrid catalytic systems as equivalent safer alternatives to concentrated sulfuric acid in nitration of aromatic compounds. *Applied Organometallic Chemistry*, 33(10): e5146, 2019.

[32] Trask, A. V., Motherwell, W. S., and Jones, W. Solvent-drop grinding: Green polymorph control of cocrystallisation. *Chemical Communications*, (7):890-891, 2004.

[33] Tanemura, K. Acceleration under solvent-drop grinding: Synthesis of bis (indolyl) methanes using small amounts of organic solvents or ionic liquids. *Tetrahedron Letters*, 82:153391, 2021.

[34] Das, S., Porashar, B., Saikia, S., and Borah, R. Brönsted acidic ionic liquids catalysed sequential Michael-like addition of indole with chalcones via Claisen-Schmidt condensation. *ChemistrySelect*, 5(10):3041-3047, 2020.

[35] Khanna, R. K. and Stranz, D. D. Infrared and Raman spectra of $KMnO_4$ complexed with 18-crown-6 ether. *Spectrochimica Acta Part A: Molecular Spectroscopy*, 36(4):387-388, 1980.

[36] Hendra, P. J. The vibrational spectrum of the permanganate ion. *Spectrochimica Acta Part A: Molecular Spectroscopy*, 24(2):125-129, 1968.

[37] Herbstein, F. H., Ron, G., and Weissman, A. The thermal decomposition of potassium permanganate and related substances. Part I. Chemical aspects. *Journal of the Chemical Society A: Inorganic, Physical, Theoretical*, 1821-1826, 1971.

[38] Viste, A. and Gray, H. B. The electronic structure of permanganate ion. *Inorganic Chemistry*, 3(8):1113-1123, 1964.

[39] Tanabe, I., Kurawaki, Y., Morisawa, Y., and Ozaki, Y. Electronic absorption spectra of imidazolium-based ionic liquids studied by far-ultraviolet spectroscopy and quantum chemical calculations. *Physical Chemistry Chemical Physics*, 18(32):22526-22530, 2016.

[40] Engert, C. and Kiefer, W. Raman spectra of the permanganate ion in the solid state with excitation in the near infrared. *Journal of Raman Spectroscopy*, 22(11):715-719, 1991.

[41] Kamimura, A., Komatsu, H., Moriyama, T., and Nozaki, Y. Sub-stoichiometric oxidation of benzylic alcohols with commercially available activated MnO_2 under oxygen atmosphere: A green modification of the benzylic oxidation. *Tetrahedron*, 69(29):5968-5972, 2013.

[42] Harding, K. E., May, L. M., and Dick, K. F. Selective oxidation of allylic alcohols with chromic acid. *The Journal of Organic Chemistry*, 40(11):1664-1665, 1975.

[43] Trahanovsky, W. S., Young, L. B., and Brown, G. L. Oxidation of organic compounds with cerium (IV). IV. Oxidation of benzyl and related alcohols. *The Journal of Organic Chemistry*, 32(12):3865-3868, 1967.

[44] Collins, J. C., Hess, W. W., and Frank, F. J. Dipyridine-chromium (VI) oxide oxidation of alcohols in dichloromethane. *Tetrahedron Letters*, 9(30):3363-3366, 1968.

[45] Becke, A. D. Density-functional thermochemistry. I. The effect of the exchange-only gradient correction. *The Journal of Chemical Physics*, 96(3):2155-2160, 1992.

[46] Lee, C., Yang, W., and Parr, R. G. Development of the Colle-Salvetti correlation-energy formula into a functional of the electron density. *Physical Review B*, 37(2):785, 1988.

[47] Frisch, M. J., Trucks, G. W., Schlegel, H. B., Scuseria, G. E., Robb, M. A., Cheeseman, J. R., Scalmani, G., Barone, V., Petersson, G. A., Nakatsuji, H., Li, X., Caricato, M., Marenich, A. V., Bloino, J., Janesko, B. G., Gomperts, R., Mennucci, B., Hratchian, H. P., Ortiz, J. V., Izmaylov, A. F., Sonnenberg, J. L., Williams-Young, D., Ding, F., Lipparini, F., Egidi, F., Goings, J., Peng, B., Petrone, A., Henderson, T., Ranasinghe, D., Zakrzewski, V. G., Gao, J., Rega, N., Zheng, G., Liang, W., Hada, M., Ehara, M., Toyota, K., Fukuda, R., Hasegawa, J., Ishida, M., Nakajima, T., Honda, Y., Kitao, O., Nakai, H., Vreven, T., Throssell, K., Montgomery Jr., J. A., Peralta, J. E., Ogliaro, F., Bearpark, M. J., Heyd, J. J., Brothers, E. N., Kudin, K. N., Staroverov, V. N., Keith, T. A., Kobayashi, R., Normand, J., Raghavachari, K., Rendell, A. P., Burant, J. C., Iyengar, S. S., Tomasi, J., Cossi, M., Millam, J. M., Klene, M., Adamo, C., Cammi, R., Ochterski, J. W., Martin, R. L., Morokuma, K., Farkas, O., Foresman, J. B., and Fox, D. J. GAUSSIAN 09 (Revision D.01), Gaussian Inc., Wallingford, CT, 2009.

[48] Mayaliwa, M., Guido, M., and Okuma Emile, K. Theoretical DFT (B3LYP)/6-31+ G (d) study on the prediction of the preferred interaction site of 3-methyl-4-pyrimidone with different proton donors. *Natural Science*, 2012, 2012.

[49] Benjamine, A. A., Mawa, K., Laye, A. L., Lucie, B. A., Soleymane, K., Robert, N. G. B., Sawaliho, B. E. H., and Thomas, N. G. Y. Density functional theory (B3LYP/6-311+ G (d, p)) study of stability, tautomerism and acidity of 2-thioxanthine in gas and aqueous phases. *International Journal of Computational and Theoretical Chemistry*, 13(2):49-55, 2019.